

# Imprints of an early matter-dominated era arising from dark matter dilution mechanism on cosmic string dynamics and gravitational wave signatures

Shi-Qi Ling and Zhao-Huan Yu\*

*School of Physics, Sun Yat-Sen University, Guangzhou 510275, China*

We investigate the influence of an early matter-dominated era in cosmic history on the dynamics of cosmic strings and the resulting stochastic gravitational waves. Specifically, we examine the case where this era originates from the dark matter dilution mechanism within the framework of the minimal left-right symmetric model. By numerically solving the Boltzmann equations governing the energy densities of the relevant components, we meticulously analyze the modifications to the cosmological scale factor, the number density of cosmic string loops, and the gravitational wave spectrum. Our results reveal that the early matter-dominated era causes a characteristic suppression in the high-frequency regime of the gravitational wave spectrum, providing distinct and testable signatures for future ground-based interferometer experiments.

## CONTENTS

I. Introduction	2
II. Gravitational waves originating from cosmic strings	3
A. Gravitational waves from cosmic string loops	3
B. Number density of cosmic string loops	5
III. Gravitational wave spectrum influenced by an early matter-dominated era	9
A. Early matter-dominated era	10
B. Dark matter dilution mechanism	10
C. Impact on the loop number density of cosmic strings	14
D. Modification of the GW spectrum	18
IV. Summary	22
Acknowledgments	23
References	23

---

\* Corresponding author. [yuzhaoh5@mail.sysu.edu.cn](mailto:yuzhaoh5@mail.sysu.edu.cn)

## I. INTRODUCTION

Modern cosmology originates from the study of the universe expansion and element formation [1]. Further observations give rise to the standard  $\Lambda$ CDM cosmological model, which suggests that after inflation and reheating, the universe successively experiences a radiation-dominated (RD) era, a matter-dominated era (MD), and a dark-energy-dominated era. Main evidences involve the observations of the cosmic expansion [2], the big bang nucleosynthesis (BBN) [3, 4], the cosmic microwave background [5–8], and the accelerating expansion at late times [9, 10].

Nevertheless, these observational results can hardly date back to pre-BBN eras. Therefore, it is essential to maintain an open perspective regarding the early history of the universe before BBN [11]. Various hypotheses beyond the standard cosmic history have been put forward, such as an early matter-dominated (EMD) era [12–19], a kination-dominated era [20–25], and an intermediate inflationary era [26–29]. Verification of such novel hypotheses about the cosmic history necessitates observational probes capable of accessing epochs prior to BBN, when the universe was opaque to photons and traditional electromagnetic detection methods are ineffective. Nonetheless, this challenge can be addressed through observations of gravitational waves (GWs), a new messenger first detected in 2015 [30]. Unlike electromagnetic radiation, GWs can propagate freely through space, preserving information from the early universe and reaching us in the present day.

To explore the pre-BBN history, the stochastic gravitational wave background (SGWB) originating from cosmic strings (CSs) provides a compelling avenue of investigation [31–42]. CSs are one-dimensional topological defects predicted by a variety of new physics theories beyond the standard model (SM), particularly those involving a spontaneously broken  $U(1)$  symmetry [43, 44]. CS loops are expected to persist as long-lasting sources, emitting GWs from their formation epoch to the present day. Once formed, the CS network rapidly evolve into a scaling regime [45–48], where their correlation length scales proportionally with the Hubble radius. As a result, the resulting SGWB spectrum encodes a wealth of information about the cosmic history. Furthermore, the SGWB generated by CSs spans an exceptionally broad frequency range, making it detectable across a diverse array of GW experiments. These include pulsar timing arrays (PTAs) operating in  $10^{-9}$ – $10^{-7}$  Hz [49–51], space-borne interferometers sensitive to  $10^{-4}$ – $10^{-1}$  Hz [52–55], and ground-based interferometers covering  $10$ – $10^3$  Hz [56–58]. Thus, future GW experiments hold immense potential to unravel the mysteries of the early universe.

In this work, we explore how the SGWB spectrum originated from a preexisting CS network is modified by an EMD era that arises within the framework of the dark matter (DM) dilution mechanism [59–68]. This mechanism addresses the DM overproduction problem by relying on significant entropy production from the decays of a long-lived particle, referred to as the “dilutor”. For the dilution mechanism to be effective, the dilutor must dominate the energy density of the universe for a finite period, thereby introducing an EMD era that interrupts the conventional RD era. To quantify the impact of this EMD era, we will trace the evolution of the total energy density of the universe by solving the relevant Boltzmann equations. This allows

us to derive the resulting SGWB spectrum, which reflects the influence of the EMD era on the cosmic string dynamics and the GW emissions.

This paper is outlined as follows. In Section II, we review the formation of CS loops and analyze their number densities during RD and MD eras, which are essential for assessing the SGWB spectrum induced by CS loops. In Section III, we investigate an EMD era emerging from the DM dilution mechanism and examine its effects on the evolution of the CS network, the loop number densities, and the resulting SGWB spectrum. Finally, in Section IV, we summarize our findings.

## II. GRAVITATIONAL WAVES ORIGINATING FROM COSMIC STRINGS

In a scalar field theory with a global or gauge  $U(1)$  symmetry, CSs could be formed after the spontaneous breaking of the  $U(1)$  symmetry in the early universe. They are one-dimensional topological defects concentrating energy of the scalar field (and the gauge field for the gauged case) [69]. In the Nambu-Goto approximation, CSs are described as infinitely thin objects with tension  $\mu$ , which is the energy per unit length. The dimensionless quantity  $G\mu$  is commonly used to represent the CS tension. Considering the dynamics of CSs, these combined factors establish CSs as promising sources of GWs [35, 70].

### A. Gravitational waves from cosmic string loops

Cosmic strings are generated randomly in the early universe, leading to the formation of a CS network. Long strings with super-horizon lengths could intersect with each other to form CS loops, whose relativistic oscillations can effectively emit GWs. Although small structures in long strings can also produce GWs, their contributions are generally negligible, compared to those generated by loops [37, 71, 72]. In practice, it is sufficient to consider only the stochastic GWs originating from CS loops.

The GW emission power of CS loops is given by [72, 73]

$$P = \Gamma G\mu^2, \quad (1)$$

where the coefficient  $\Gamma$  is estimated to be about 50 [74], and  $G$  represents the Newtonian gravitational constant. The frequencies of GWs emitted by a CS loop of length  $l$  are [70]

$$f_e = \frac{2n}{l}, \quad n \in \mathbb{N}^+, \quad (2)$$

where  $n$  denotes the harmonic modes of the loop oscillation. Thus, the expression for the power can be rewritten as

$$P = G\mu^2 \sum_n P_n, \quad (3)$$

where  $P_n$  is the dimensionless emission power in units of  $G\mu^2$  for a single mode  $n$ , which can be estimated by numerical simulations for GW emissions in RD and MD eras [74].

Introducing  $n_{\text{CS}}(l, t) dl$  as the number density of CS loops of length  $l$  at cosmic time  $t$ , the energy density of GWs emitted from CS loops per unit time at the emission time  $t_e$  can be expressed as

$$\left. \frac{d\rho_{\text{GW}}}{dt} \right|_{t_e} = G\mu^2 \sum_n P_n \int_0^{l_{\text{max}}} n_{\text{CS}}(l, t_e) dl. \quad (4)$$

Using Eq. (2), we derive

$$\left. \frac{d^2\rho_{\text{GW}}}{dt df} \right|_{t_e} = G\mu^2 \sum_n \frac{2nP_n}{f_e^2} n_{\text{CS}}\left(\frac{2n}{f_e}, t_e\right). \quad (5)$$

Note that this result corresponds to the GW emission time  $t_e$ , but GW experiments only receive signals at the present time  $t_0$ . Hence, the effect of the cosmological redshift must be accounted for, and the present GW frequency is given by  $f = a(t_e)f_e$ , while the present GW energy density is  $\rho_{\text{GW}} = \rho_{\text{GW}}(t_e)a^4(t_e)$ , where  $a(t)$  is the scale factor normalized such that  $a(t_0) = 1$ . Integrating Eq. (5) over time, we arrive at

$$\frac{d\rho_{\text{GW}}}{df} = G\mu^2 \sum_n P_n C_n(f), \quad (6)$$

where

$$C_n(f) = \frac{2n}{f^2} \int_{t_*}^{t_0} a^5(t) n_{\text{CS}}\left(\frac{2na(t)}{f}, t\right) dt, \quad (7)$$

with  $t_*$  denoting the cosmic time when CS loops start to radiate GWs.

The frequency spectrum of the SGWB induced by CS loops is commonly characterized by a dimensionless quantity

$$\Omega_{\text{GW}}(f) \equiv \frac{1}{\rho_c} \frac{d\rho_{\text{GW}}}{d \ln f} = \frac{8\pi G^2 \mu^2 f}{3H_0^2} \sum_n P_n C_n(f), \quad (8)$$

where  $\rho_c = 3H_0^2/(8\pi G)$  is the present critical density and  $H_0 = 100h \text{ km s}^{-1} \text{ Mpc}^{-1}$  is the Hubble constant with  $h = 0.674 \pm 0.005$  [8]. In order to calculate Eq. (8), we need to know the evolution of the scalar factor  $a(t)$ , which can be computed from

$$\frac{da(t)}{dt} = a(t)H(t), \quad (9)$$

where  $H(t)$  is the Hubble expansion rate.

In the standard  $\Lambda$ CDM model, the Hubble rate can be expressed as [75]

$$H = H_0 \sqrt{\Omega_r \mathcal{G}(z) a^{-4} + \Omega_m a^{-3} + \Omega_\Lambda}, \quad (10)$$

where  $z = a^{-1} - 1$  is the cosmological redshift.  $\Omega_r = 1.68 \times (5.38 \pm 0.15) \times 10^{-5}$ ,  $\Omega_m = 0.315 \pm 0.007$ , and  $\Omega_\Lambda = 0.685 \pm 0.007$  [76] are cosmological constants representing the energy fraction of radiation, matter, and dark energy, respectively.

$$\mathcal{G}(z) = \frac{g_\star(z)g_{\star s}^{4/3}(0)}{g_\star(0)g_{\star s}^{4/3}(z)} \quad (11)$$

is a function of the redshift  $z$  introduced to account for the changes in relativistic degrees of freedom, where  $g_\star(z)$  and  $g_{\star s}(z)$  are the effective numbers of relativistic degrees of freedom for the energy and entropy densities, respectively. Considering the evolution of  $g_\star(z)$  and  $g_{\star s}(z)$ , we can approximate  $\mathcal{G}(z)$  as a piecewise function which changes its value at the epochs of electron-positron annihilation ( $z \simeq 10^9$ ) and QCD phase transition ( $z \simeq 2 \times 10^{12}$ ): [75]

$$\mathcal{G}(z) = \begin{cases} 1, & z < 10^9, \\ 0.83, & 10^9 < z < 2 \times 10^{12}, \\ 0.39, & z > 2 \times 10^{12}. \end{cases} \quad (12)$$

However, if an EMD era exists, the evolution of the Hubble rate  $H(t)$  would be altered, necessitating modifications to the expressions above. This situation will be discussed in detail in Section III.

## B. Number density of cosmic string loops

The evolution of the CS network can be appropriately described using the velocity-dependent one-scale (VOS) model [72, 77, 78], where the correlation length  $L$  and the root-mean-square (RMS) velocity  $v$  of string segments serve as two fundamental parameters characterizing the dynamics of the network. Thus, the energy density of long strings can be expressed as  $\rho = \mu/L^2$ , and its evolution in the universe is governed by [77]

$$\dot{\rho} = -2H(1 + v^2)\rho - \frac{\tilde{c}v}{L}\rho, \quad (13)$$

where the friction effect is neglected. The term  $-2H\rho$  accounts for the dilution and stretching of the strings due to the cosmic expansion, while the term  $-2Hv^2\rho$  captures the energy loss caused by the redshifting of velocities. The term  $-\tilde{c}v\rho/L$  represents the energy removed through loop formation, where  $\tilde{c} \simeq 0.23$  [79] is the loop chopping efficiency. Additionally, the evolution of the RMS velocity  $v$  is determined by [77]

$$\dot{v} = (1 - v^2) \left[ \frac{k(v)}{L} - 2Hv \right] \quad (14)$$

with [79]

$$k(v) = \frac{2\sqrt{2}}{\pi}(1-v^2)(1+2\sqrt{2}v^3)\frac{1-8v^6}{1+8v^6}. \quad (15)$$

Introducing a dimensionless quantity  $\xi \equiv L/t$ , which represents the correlation length  $L$  normalized by the cosmic time  $t$ , the evolution equations above can be rewritten as

$$t\dot{\xi} = H(1+v^2)t\xi - \xi + \frac{1}{2}\tilde{c}v, \quad (16)$$

$$t\dot{v} = (1-v^2) \left[ \frac{k(v)}{\xi} - 2Htv \right]. \quad (17)$$

By numerically solving these equations, one finds that the solutions rapidly converge to constant values of  $\xi$  and  $v$ , independent of the initial conditions. This indicates that the CS network quickly evolves into a linear scaling regime characterized by  $L \propto t$ . By setting  $\dot{\xi} = \dot{v} = 0$ , the scaling solutions for RD and MD eras can be derived as [80]

$$\xi_r = 0.271, \quad v_r = 0.662, \quad \text{RD era}, \quad (18)$$

$$\xi_m = 0.625, \quad v_m = 0.582, \quad \text{MD era}. \quad (19)$$

The increase in the energy density of CS loops  $\rho_o$  is driven by the energy transfer from long strings, expressed as [37, 80, 81]

$$\dot{\rho}_o = \frac{\mathcal{F}}{\gamma_v} \frac{\tilde{c}v}{L} \rho = \frac{\mathcal{F}\tilde{c}v\mu}{\gamma_v \xi^3 t^3}, \quad (20)$$

where the Lorentz factor  $\gamma_v \equiv (1-v^2)^{-1/2}$  incorporates the energy loss caused by the redshifting of the loop velocity, and  $\mathcal{F}$  is a coefficient that characterizes the fraction of slow, large loops responsible for the dominant contribution to GW emissions. The values of  $\mathcal{F}$  differ between RD and MD eras, denoted as  $\mathcal{F}_r$  and  $\mathcal{F}_m$ , respectively. These values can be determined by comparison with numerical simulations in the scaling regime [82, 83].

The energy in a CS loop of length  $l$  is expressed as  $\mu l$ . Thus, the loop production function, defined by [37, 80]

$$\mathcal{P}(l, t) = \frac{1}{\mu l} \frac{d\rho_o}{dl}, \quad (21)$$

quantifies the rate of increase in the number density of CS loops per unit length per unit time. Because of GW emission, a CS loop of length  $l'$  at time  $t'$  loses energy  $\Gamma G\mu^2(t-t')$  by time  $t$  and consequently shrinks to a length  $l = l' - \Gamma G\mu(t-t')$ . Therefore, the loop number density per unit loop length at time  $t$  is given by

$$n_{\text{CS}}(l, t) = \frac{1}{a^3(t)} \int_{t_{\text{ini}}}^t \mathcal{P}(l', t') a^3(t') dt', \quad (22)$$

with  $l'(t) = l + \Gamma G\mu(t - t_{\text{ini}})$ .  $t_{\text{ini}}$  denotes the initial time of loop production, and the scale factors account for the dilution because of cosmic expansion. To determine  $n_{\text{CS}}(l, t)$  for calculating the energy density of emitted GWs according to Eq. (4), knowledge of the loop production function  $\mathcal{P}(l, t)$  is required.

During an RD era, numerical simulations [83] reveal that most large loops are generated with a length  $l$  characterized by a fraction  $\alpha_r = l/L$  of the correlation length  $L$ .  $\alpha_r$  satisfies  $\alpha_r \xi_\star \simeq 0.1$ , where a quantity with a subscript  $\star$  is evaluated at the loop production time  $t_\star$ . Consequently, the loop production function can be accurately approximated by

$$\mathcal{P}_r(l, t) = \frac{\mathcal{F}_r \tilde{c} v}{\gamma_v \alpha_r \xi_\star^4 t^5} \delta\left(\alpha_r \xi - \frac{l}{t}\right), \quad \text{RD era}, \quad (23)$$

where  $\delta(x)$  denotes the Dirac  $\delta$  function, which fixes the loop production time  $t_\star$  through the relation  $\alpha_r \xi_\star = l_\star/t_\star$ . Substituting the expression for  $\mathcal{P}_r(l, t)$  into Eq. (22) with  $a \propto t^{1/2}$  in the RD era, we derive an analytical expression for the loop number density [80, 81, 84],

$$n_{\text{CS}}^r(l, t) = \frac{\mathcal{F}_r \tilde{c} v_\star}{t^4 \gamma_{v_\star} \alpha \xi_\star^4} \frac{\Theta(\alpha \xi_\star - l/t)}{\alpha \xi_\star + \alpha \dot{\xi}_\star t_\star + \Gamma G\mu} \left(\frac{t}{t_\star}\right)^{5/2}, \quad \text{RD era}, \quad (24)$$

where  $\Theta(x)$  represents the Heaviside step function. By accounting for the decrease in loop length due to GW emission, we have  $\alpha_r \xi_\star t_\star = l_\star = l + \Gamma G\mu(t - t_\star)$ , leading to

$$t_\star = \frac{l + \Gamma G\mu t}{\alpha_r \xi_\star + \Gamma G\mu}. \quad (25)$$

In the scaling regime of the RD era, we have  $\xi_\star = \xi_r$ ,  $v_\star = v_r$ , and  $\dot{\xi}_\star = 0$ . Adopting

$$\mathcal{F}_r = 0.1, \quad (26)$$

the loop number density formed in an RD era for  $\alpha_r \xi_\star = 0.1 \gg \Gamma G\mu$  reduces to

$$n_{\text{CS}}^r(l, t) \simeq \frac{0.18}{t^{3/2}(l + \Gamma G\mu t)^{5/2}} \Theta(0.1t - l), \quad \text{scaling, RD era}, \quad (27)$$

which agrees with the result from numerical simulations presented in Ref. [83].

On the other hand, numerical simulations for an MD era suggest that loop production occurs on a wider range of scales compared to that in an RD era and can be effectively described by a power-law distribution of  $l^{-1.69}$  with a cutoff [83]. This motivate us to assume the loop production function as

$$\mathcal{P}_m(l, t) = \frac{\mathcal{F}_m \tilde{c} v}{\gamma_v (l/t)^{1.69} \xi^3 t^5} \Theta\left(\alpha_m \xi - \frac{l}{t}\right), \quad \text{MD era}, \quad (28)$$

where the theta function gives a cutoff at  $l = \alpha_m L$  with  $\alpha_m$  satisfying  $\alpha_m \xi_\star \simeq 0.18$  [83]. Using

$a \propto t^{2/3}$  in the MD era, we derive the loop number density

$$n_{\text{CS}}^{\text{m}}(l, t) = \frac{\mathcal{F}_{\text{m}} \tilde{c}}{t^2} \int_{t_{\text{m}}}^t \frac{v'}{\gamma_{v'} \xi'^3 l'^{1.69} t'^{1.31}} \Theta \left( t' - \frac{l'}{\alpha_{\text{m}} \xi} \right) dt', \quad (29)$$

where  $t_{\text{m}}$  is the initial time of the MD era. Under the assumption that the  $t'$ -dependence of  $\xi'$  and  $v'$  is negligible and that  $l' = l + \Gamma G \mu (t - t') \simeq l$  for  $\Gamma G \mu \ll l/(t - t')$ , we perform integration by parts to obtain

$$\begin{aligned} n_{\text{CS}}^{\text{m}}(l, t) &\simeq \frac{\mathcal{F}_{\text{m}} \tilde{c}}{t^2} \left[ -\frac{v'}{0.31 \gamma_{v'} \xi'^3 l'^{1.69} t'^{0.31}} \Big|_{t_{\text{m}}}^t + \int_{t_{\text{m}}}^t \frac{v' \delta[t' - l'/(\alpha_{\text{m}} \xi)] dt'}{0.31 \gamma_{v'} \xi'^3 l'^{1.69} t'^{0.31}} \right] \Theta \left( t - \frac{l}{\alpha_{\text{m}} \xi} \right) \\ &= \frac{\mathcal{F}_{\text{m}} \tilde{c}}{0.31 t^2} \left[ -\frac{v}{\gamma_v \xi^3 l^{1.69} t^{0.31}} + \frac{v_{\star}}{\gamma_{v_{\star}} \xi_{\star}^3 l_{\star}^{1.69} t_{\star}^{0.31}} \right] \Theta \left( t - \frac{l}{\alpha_{\text{m}} \xi_{\star}} \right) \\ &\quad + \frac{\mathcal{F}_{\text{m}} \tilde{c}}{0.31 t^2} \frac{v(t_{\text{m}})}{\gamma_{v(t_{\text{m}})} \xi^3(t_{\text{m}}) [l + \Gamma G \mu (t - t_{\text{m}})]^{1.69} t_{\text{m}}^{0.31}} \Theta \left( t_{\text{m}} - \frac{l + \Gamma G \mu (t - t_{\text{m}})}{\alpha_{\text{m}} \xi_{\star}} \right), \quad (30) \end{aligned}$$

where  $t_{\star}$  is determined by  $\alpha_{\text{m}} \xi_{\star} t_{\star} = l + \Gamma G \mu (t - t_{\star})$ . For  $t \gg t_{\text{m}}$ , the last term in the above expression can be omitted, leading to

$$n_{\text{CS}}^{\text{m}}(l, t) \simeq \frac{\mathcal{F}_{\text{m}} \tilde{c}}{0.31 t^2} \left[ -\frac{v}{\gamma_v \xi^3 l^{1.69} t^{0.31}} + \frac{v_{\star}}{\gamma_{v_{\star}} \xi_{\star}^3 l_{\star}^{1.69} t_{\star}^{0.31}} \right] \Theta \left( t - \frac{l}{\alpha_{\text{m}} \xi_{\star}} \right). \quad (31)$$

Moreover, for small  $\Gamma G \mu$ , we can use the approximations  $t_{\star} \simeq (\alpha_{\text{m}} \xi_{\star})^{-1} (l + \Gamma G \mu)$  and  $t' \simeq (l/t')^{-1} (l + \Gamma G \mu)$  to express the loop number density in the MD era as

$$n_{\text{CS}}^{\text{m}}(l, t) \simeq \frac{\mathcal{F}_{\text{m}} \tilde{c}}{0.31 t^2 (l + \Gamma G \mu t)^2} \left[ \frac{v_{\star} (\alpha_{\text{m}} \xi_{\star})^{0.31}}{\gamma_{v_{\star}} \xi_{\star}^3} - \frac{v (l/t)^{0.31}}{\gamma_v \xi^3} \right] \Theta \left( \alpha_{\text{m}} \xi_{\star} - \frac{l}{t} \right), \quad \text{MD era.} \quad (32)$$

In the scaling regime, where  $\xi = \xi_{\star} = \xi_{\text{m}}$  and  $v = v_{\star} = v_{\text{m}}$ , taking  $\alpha_{\text{m}} \xi_{\star} = 0.18$  and

$$\mathcal{F}_{\text{m}} = 0.316, \quad (33)$$

the loop number density formed in the MD era becomes

$$n_{\text{CS}}^{\text{m}}(l, t) = \frac{0.27 - 0.45 (l/t)^{0.31}}{t^2 (l + \Gamma G \mu t)^2} \Theta(0.18 t - l), \quad \text{scaling, MD era,} \quad (34)$$

which is also consistent with the simulation result in Ref. [83].

We now analyze the SGWB spectrum generated by CS loops within the standard  $\Lambda$ CDM cosmological model, utilizing the expressions (27) and (34) for the loop number density in the scaling regime. In the  $\Lambda$ CDM model, the MD era succeeds the RD era at the time of matter-radiation equality,  $t_{\text{eq}} = 51.1 \pm 0.8 \text{ kyr}$  [76]. Notably, CS loops formed during the RD era and surviving into the MD era also contribute to the loop number density in the MD era, as given

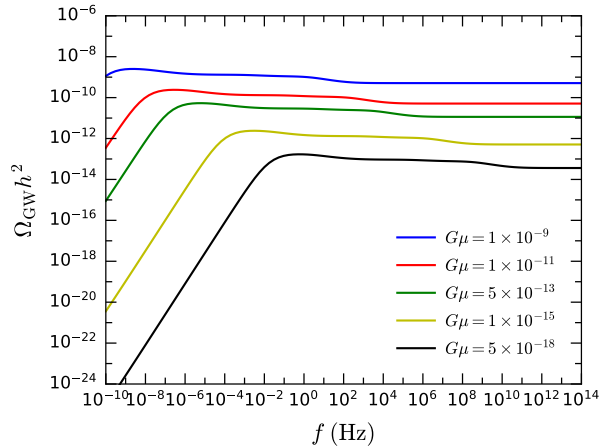


FIG. 1. SGWB spectra for various values of  $G\mu$  in the standard  $\Lambda$ CDM cosmological model.

by [83]

$$n_{\text{CS}}^{\text{rm}}(l, t) = \frac{0.18 t_{\text{eq}}^{1/2}}{t^2 (l + \Gamma G\mu t)^{5/2}} \Theta(0.1 t_{\text{eq}} - l - \Gamma G\mu t), \quad \text{scaling.} \quad (35)$$

By inserting the scale factor  $a(t)$  and the loop number density  $n_{\text{CS}}(l, t)$  into Eqs. (7) and (8), the SGWB spectrum can be obtained.

In Fig. 1, we demonstrate the SGWB spectra in the  $\Lambda$ CDM model for the CS tension parameter  $G\mu = 10^{-9}, 10^{-11}, 5 \times 10^{-13}, 10^{-15}$ , and  $5 \times 10^{-18}$ . At sufficiently high frequencies, the spectra tend to be flat, primarily due to GW emissions during the RD era [83]. For smaller values of  $G\mu$ , the total GW emission power is reduced, allowing CS loops to survive longer. At a specific cosmic time, the average length of loops would be smaller, leading to GWs emitted at higher frequencies. As a result, the SGWB spectrum shifts downward in amplitude and rightward in frequency as  $G\mu$  decreases [74].

In the following section, we will examine the effects of an additional EMD era inserted into the RD era, focusing on its impact on the scale factor, the loop number density, and the SGWB spectrum. This modification may violate the scaling behavior, necessitating the use of the more general expressions for the loop number density as in Eqs. (24) and (32).

### III. GRAVITATIONAL WAVE SPECTRUM INFLUENCED BY AN EARLY MATTER-DOMINATED ERA

In this section, we discuss an EMD era motivated by the DM dilution mechanism and study its impact on the SGWB spectrum generated by cosmic strings.



FIG. 2. Sketch of the cosmic timeline featuring an EMD era. In chronological order, the universe evolves through the original RD era, the EMD era, the second RD era, and the final MD era.

### A. Early matter-dominated era

An EMD era is an MD period spanning from cosmic time  $t_1$  to  $t_2$ , embedded within the conventional RD era. Thus, there exists an initial RD era before  $t_1$ , and a subsequent RD era after  $t_2$ . The second RD era ends at the time of matter-radiation equality  $t_{\text{eq}}$ , after which the universe transitions into the final MD era, corresponding to the traditional cosmological evolution. This timeline is depicted in Fig. 2.

We propose the following assumption for the origin of such an EMD era. A massive, long-lived particle  $Y$  decouples from thermal equilibrium and transitions into nonrelativistic matter, dominating the universe as the temperature decreases and initiating an EMD era at time  $t_1$ . The slow decays of  $Y$  into SM particles release entropy into the plasma. In the context of the DM dilution mechanism, this entropy injection dilutes the DM abundance to the observed value. Once the majority of  $Y$  particles have decayed, the EMD era concludes at time  $t_2$ .

Now we discuss the evolution of the related energy densities. The radiation and matter energy densities,  $\rho_r$  and  $\rho_m$ , scale with the scale factor  $a$  as [85]

$$\rho_r \propto a^{-4}, \quad \rho_m \propto a^{-3}. \quad (36)$$

The scale factor evolves as  $a \propto t^{1/2}$  in an RD era and  $a \propto t^{2/3}$  in an MD era. Starting from an initial temperature  $T_{\text{ini}}$  in the original RD era, the  $Y$  particles constitute a matter component with energy density  $\rho_Y$ , while the plasma of SM particles has energy density  $\rho_{\text{SM}}$ . Consequently, the energy densities evolve as

$$\rho_{\text{SM}} \propto t^{-2}, \quad \rho_Y \propto t^{-3/2}, \quad (37)$$

during the original RD era, and

$$\rho_{\text{SM}} \propto t^{-8/3}, \quad \rho_Y \propto t^{-2}, \quad (38)$$

during the EMD era. Notably, the energy density of  $Y$  decreases more slowly than that of SM particles during the original RD era, leading to the onset of the EMD era.

### B. Dark matter dilution mechanism

In this subsection, we discuss the DM dilution mechanism as the origin of the EMD era. As severe constraints from DM detection experiments have reduced interest in weakly interacting

massive particles with masses around the electroweak scale as DM candidates, a lighter DM candidate  $X$  has gained prominence due to its ability to evade direct detection bounds. Nevertheless, thermal production of  $X$  particles with low annihilation cross sections typically results in an overproduction problem [86, 87]. Within the DM dilution mechanism [60–64, 66, 67], the overproduction of DM particles is mitigated by entropy injection from the decays of a dilutor particle  $Y$ , which dominates the universe for a period, thereby inducing an EMD era.

Following Ref. [68], we discuss the DM dilution mechanism within the minimal left-right symmetric model (LRSM) as a concrete and illustrative example. In this model, the lightest right-handed neutrino  $N_1$  serves as the light DM candidate  $X$ , and the next-to-lightest right-handed neutrino  $N_2$  or a neutral Higgs boson  $\Delta$  acts as the dilutor  $Y$ . As a Majorana fermion, the DM candidate  $X$  has two degrees of freedom and its number density in thermal equilibrium and in the relativistic limit is given by [85]

$$n_X = \frac{3\zeta(3)}{2\pi^2} T^3. \quad (39)$$

where  $T$  denotes the temperature and  $\zeta(x)$  represents the Riemann zeta function. For sufficiently weak interactions,  $X$  particles freeze out from the plasma at a temperature  $T_{\text{FO}} \gg m_X$ , leaving a number density in the comoving volume of

$$Y_X \equiv \frac{n_X}{s} = \frac{135\zeta(3)}{4\pi^4 g_{*s}(T_{\text{FO}})}, \quad (40)$$

where  $s = 2\pi^2 g_{*s}(T) T^3/45$  is the entropy density.

If  $X$  particles evolve without interference,  $Y_X$  remains conserved, leading to a present-day relic energy density fraction of [68]

$$\Omega_X^0 = \frac{m_X Y_X s_0}{\rho_c} \simeq 2.6 \frac{m_X}{\text{keV}} \frac{100}{g_{*s}(T_{\text{FO}})}, \quad (41)$$

where  $s_0 = 2891.2 \text{ cm}^{-3}$  and  $\rho_c = 1.05 \times 10^{-5} h^2 \text{ GeV/cm}^3$  [76] are the entropy density and the critical energy density at present, respectively. Thus, for  $m_X \lesssim \text{keV}$ ,  $\Omega_X^0$  exceeds the observed cold DM relic density  $\Omega_{\text{CDM}} = 0.265$  [76] by at least one order of magnitude, causing an overproduction problem.

Introducing a long-lived dilutor  $Y$  with a mass  $m_Y$  much larger than  $m_X$  can effectively address the overproduction problem of  $X$  particles. First, during the RD era, both  $Y$  and  $X$  particles decouple relativistically at a similar temperature, resulting in comparable yields,  $Y_Y \simeq Y_X$ . Second, because of  $m_Y \gg m_X$ ,  $Y$  particles become nonrelativistic at a relatively high temperature, while  $X$  particles remain relativistic. Consequently,  $Y$  particles quickly dominate the energy density of the universe, initiating an EMD era. Finally, when the lifetime of  $Y$  particles comes to an end, they decay into SM particles and  $X$  particles, injecting entropy and consequently diluting the energy density  $\rho_X$  of  $X$  particles.

This situation can be analyzed using the Boltzmann equations [67]

$$\frac{d\rho_Y}{dt} + 3H\rho_Y = -\Gamma_Y\rho_Y, \quad (42)$$

$$\frac{d\rho_X}{dt} + 4H\rho_X = yB_X\Gamma_Y\rho_Y, \quad (43)$$

$$\frac{d\rho_{\text{SM}}}{dt} + 4H\rho_{\text{SM}} = (1 - yB_X)\Gamma_Y\rho_Y, \quad (44)$$

where  $\Gamma_Y$  is the decay width of the dilutor  $Y$ ,  $y$  represents the energy fraction carried away by  $X$  particles among all the decay products of  $Y$ , and  $B_X$  is the branching ratio of the decay channel  $Y \rightarrow X$ . Assuming that  $X$  particles remain ultra-relativistic throughout the aforementioned process, and using

$$H = \sqrt{\frac{8\pi}{3M_{\text{Pl}}^2}(\rho_X + \rho_Y + \rho_{\text{SM}})}, \quad (45)$$

we can solve the Boltzmann equations.

In the minimal LRSM with the  $\text{SU}(3)_C \times \text{SU}(2)_L \times \text{SU}(2)_R \times \text{U}(1)_{B-L}$  gauge symmetry [88, 89] considered in Ref. [68], there are two scenarios for the DM dilution mechanism, where the DM candidate  $X$  is the lightest right-handed neutrino  $N_1$ .

- Scenario 1: the dilutor  $Y$  is the next-to-lightest right-handed neutrino  $N_2$ , which undergoes a three-body decay mediated by a right-handed gauge boson  $W_R^\pm$  into two charged leptons  $\ell\ell'$  and one  $N_1$ . The related right-handed charged current interactions are described by the Lagrangian

$$\mathcal{L}_1 = \frac{g}{\sqrt{2}}W_R^\mu \left( \sum_{i=1}^2 \bar{N}_i \gamma_\mu V_{\text{PMNS}}^{R\dagger} \ell_R + \bar{u}_R \gamma_\mu V_{\text{CKM}}^R d_R \right) + \text{H.c.}, \quad (46)$$

where  $g$  is the unified  $\text{SU}(2)_L \times \text{SU}(2)_R$  gauge coupling, and  $V_{\text{PMNS}}^R$  and  $V_{\text{CKM}}^R$  are the right-handed Pontecorvo-Maki-Nakagawa-Sakata (PMNS) and Cabibbo-Kobayashi-Maskawa (CKM) matrices that connect the flavor and mass bases. The decay channels of  $Y$  include  $N_2 \rightarrow N_1\ell\ell'$ ,  $N_2 \rightarrow \ell q\bar{q}'$ , and  $N_2 \rightarrow \ell W$ .

- Scenario 2: the dilutor  $Y$  is the neutral Higgs boson  $\Delta$ , which is associated with the origin of the Majorana neutrino masses and can decay into two  $N_1$  particles. The relevant Yukawa couplings are given by the Lagrangian

$$\mathcal{L}_2 = \bar{Q}_L(Y_q\Phi + \tilde{Y}_q\tilde{\Phi})Q_R + \bar{L}_L(Y_l\Phi + \tilde{Y}_l\tilde{\Phi})L_R + Y_{\Delta_L}L_L^T i\sigma_2 \Delta_L L_L + Y_{\Delta_R}L_R^T i\sigma_2 \Delta_R L_R + \text{H.c.}, \quad (47)$$

where the family indices are suppressed.  $\Phi$  is an  $\text{SU}(2)_L \times \text{SU}(2)_R$  bidoublet scalar, with  $\tilde{\Phi} = i\sigma_2\Phi^*i\sigma_2$ .  $\Delta_L$  and  $\Delta_R$  are  $\text{SU}(2)_L$  and  $\text{SU}(2)_R$  triplet scalars, respectively.  $Q_{L,R}$  and  $L_{L,R}$  denote left-handed and right-handed quarks and leptons.  $Y_q, \tilde{Y}_q, Y_l, \tilde{Y}_l, Y_{\Delta_L}$ , and  $Y_{\Delta_R}$  represent the Yukawa coupling matrices. The dilutor  $\Delta$  is the Higgs boson arising

TABLE I. Benchmark points in Scenario 1 where  $N_2$  serves as the dilutor  $Y$ .

Scenario 1	BP1a	BP1b	BP1c
Common	$m_{N_2} = 200 \text{ GeV}, y = 0.35, \tan \beta = 0.5$		
$m_{N_1}$	6.5 keV	10 keV	30 keV
$m_{W_R}$	$5 \times 10^7 \text{ GeV}$	$6 \times 10^7 \text{ GeV}$	$7 \times 10^7 \text{ GeV}$
$\Gamma_Y$	$2.22 \times 10^{-23} \text{ GeV}$	$1.07 \times 10^{-23} \text{ GeV}$	$5.77 \times 10^{-24} \text{ GeV}$
$B_X$	$4.41 \times 10^{-3}$	$4.41 \times 10^{-3}$	$4.41 \times 10^{-3}$

TABLE II. Benchmark points in Scenario 2 where  $\Delta$  serves as the dilutor  $Y$ .

Scenario 2	BP2a	BP2b	BP2c
Common	$m_{N_1} = 6.5 \text{ keV}, y = 1, \theta_{\Delta h} = 0$		
$m_{\Delta}$	1 TeV	$10^3 \text{ TeV}$	$10^6 \text{ TeV}$
$m_{W_R}$	$10^{11} \text{ GeV}$	$3.16 \times 10^{12} \text{ GeV}$	$10^{14} \text{ GeV}$
$\Gamma_Y$	$3.51 \times 10^{-21} \text{ GeV}$	$3.51 \times 10^{-15} \text{ GeV}$	$3.51 \times 10^{-9} \text{ GeV}$
$B_X$	$5.11 \times 10^{-12}$	$5.11 \times 10^{-18}$	$2.42 \times 10^{-20}$

from the electrically neutral component of  $\Delta_R$ . Its decay channels involve  $\Delta \rightarrow N_1 N_1$ ,  $\Delta \rightarrow W_R^* W_R^* \rightarrow 4 \text{ fermions}$ ,  $\Delta \rightarrow \gamma\gamma$ , and so on.

We will consider both scenarios in the following analysis.

We solve the Boltzmann equations for the benchmark points (BPs) specified in Tables I and II for Scenarios 1 and 2, respectively. The values of  $y$ ,  $m_{N_1}$ ,  $m_{N_2}$ ,  $m_{\Delta}$ ,  $m_{W_R}$ , the ratio  $\tan \beta$  of two vacuum expectation values from the bidoublet, and the mixing angle  $\theta_{\Delta h}$  between  $\Delta$  and the 125 GeV Higgs boson  $h$  are adopted based on the results presented in Ref. [68]. The dilutor decay width  $\Gamma_Y$  and the branching ratio  $B_X$  are calculated using the formulas provided therein. All BPs are selected to ensure the correct DM relic abundance through the DM dilution mechanism. BP1a and BP2a will be the primary focus of the following analysis, while the remaining BPs will provide additional results for comparison.

We adopt the initial temperature as  $T_{\text{ini}} = m_Y/10$ , at which  $Y$  particles have decoupled with  $Y_Y \simeq Y_X$  and become nonrelativistic, while  $X$  particles are relativistic. The initial conditions for the energy densities of  $Y$ ,  $X$ , and SM particles are

$$\rho_Y^{\text{ini}} = m_Y Y_Y s(T_{\text{ini}}) \simeq \frac{2\pi^2}{45} m_Y Y_X g_{\star}(T_{\text{ini}}) T_{\text{ini}}^3, \quad (48)$$

$$\rho_X^{\text{ini}} = \frac{7\pi^2}{120} T_{\text{ini}}^4, \quad (49)$$

$$\rho_{\text{SM}}^{\text{ini}} = \frac{\pi^2}{30} g_{\star}(T_{\text{ini}}) T_{\text{ini}}^4. \quad (50)$$

The obtained energy densities  $\rho_Y$ ,  $\rho_X$ , and  $\rho_{\text{SM}}$  as functions of cosmic time  $t$  are illustrated in

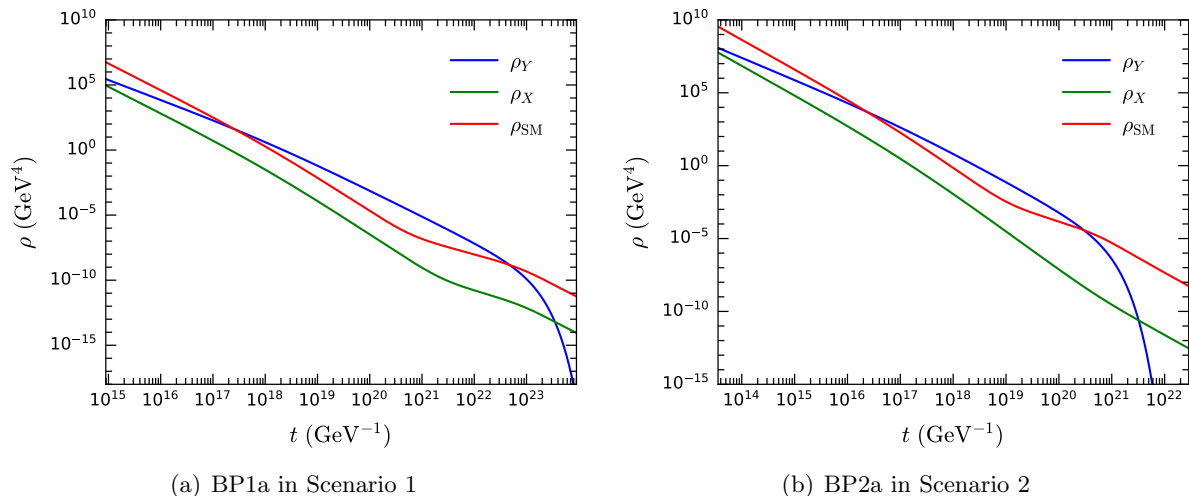


FIG. 3. Evolution of the energy densities  $\rho_Y$ ,  $\rho_X$ , and  $\rho_{\text{SM}}$  for BP1a in Scenario 1 with the dilutor  $N_2$  (a) and BP2a in Scenario 2 with the dilutor  $\Delta$  (b).

Fig. 3 for BP1a in Scenario 1 and BP2a in Scenario 2.

As we can see from Figs. 3(a) and 3(b), the initial energy density of the dilutor  $Y$  in both BPs is lower than  $\rho_{\text{SM}}$  by one order of magnitude. Nonetheless, the decrease in  $\rho_Y$  is slower than that of  $\rho_{\text{SM}}$  as the universe expands, leading to  $\rho_Y = \rho_{\text{SM}}$  at  $t_1 \simeq 3 \times 10^{17} \text{ GeV}^{-1}$  and  $t_1 \simeq 2 \times 10^{16} \text{ GeV}^{-1}$  in BP1a and BP2a, respectively. This indicates the beginning of the EMD era. Subsequently,  $Y$  particles dominate the universe until their decays become effective, leading to the end of the EMD era at  $t_2 \simeq 5 \times 10^{22} \text{ GeV}^{-1}$  for BP1a and  $t_2 \simeq 3 \times 10^{20} \text{ GeV}^{-1}$  for BP2a. Since  $\Gamma_Y$  in BP1a is lower than that in BP2a, as shown in Tables I and II, the decays of  $Y$  particles occur at later times, leading to a longer duration of the EMD era. The  $Y$  decays inject entropy into the plasma, increasing  $\rho_{\text{SM}}$ , the plasma temperature, and the entropy density  $s$ . Consequently, the  $X$  comoving number density  $Y_X = n_X/s$  is significantly diluted, ensuring that the relic abundance of  $X$  particles being consistent with the observation in both BPs.

By substituting the obtained  $\rho_Y$ ,  $\rho_X$ , and  $\rho_{\text{SM}}$  into Eq. (45) and solving Eq. (9) with  $a(t_0) = 1$ , we determine the evolution of the scale factor  $a(t)$  in both BPs, as illustrated in Fig. 4. Compared with the standard  $\Lambda\text{CDM}$  cosmological model, the presence of the EMD era reduces the scale factor prior to  $t_2$ . This occurs because the scale factor evolves as  $a \propto t^{2/3}$  during an MD era, increasing more rapidly with time than  $a \propto t^{1/2}$  during an RD era. Therefore, and a smaller  $a$  is required at the onset of the EMD era to ensure  $a(t_0) = 1$  at the present time  $t_0$ .

### C. Impact on the loop number density of cosmic strings

Since the insertion of the EMD era affects the evolution of the CS network in the VOS model, it is necessary to examine how the normalized correlation length  $\xi$  and the RMS velocity  $v$  change with time. We should consider these variations when calculating the number density of CS loops during the EMD era. To achieve this, we solve Eqs. (16) and (17) with the Hubble rate

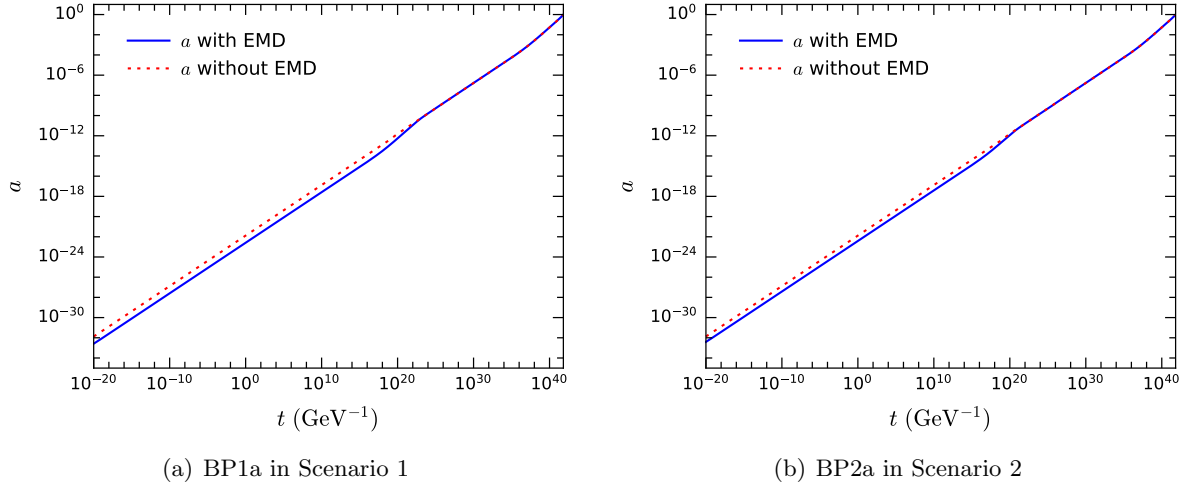


FIG. 4. Evolution of the scale factor  $a(t)$  (blue solid lines) for BP1a in Scenario 1 with the dilutor  $N_2$  (a) and BP2a in Scenario 2 with the dilutor  $\Delta$  (b). For comparison, the result from the standard  $\Lambda$ CDM model, which does not include the EMD era, is represented by red dotted lines.

$H(t)$  modified by the presence of the EMD era, and obtain  $\xi$  and  $v$  being functions of cosmic time  $t$  for BP1a and BP2a, as demonstrated by blue solid lines in Fig. 5. For comparison, the results of the standard  $\Lambda$ CDM model without the EMD era are also presented as red dotted lines.

During the RD era in the  $\Lambda$ CDM model,  $\xi$  and  $v$  basically maintain the scaling values  $\xi_r = 0.271$  and  $v_r = 0.662$ , as stated in Eq. (18). Some deviations around  $t \sim 10^{20} \text{ GeV}^{-1}$  and  $t \sim 10^{26} \text{ GeV}^{-1}$  are attributed to changes in relativistic degrees of freedom shown in Eq. (12). For  $t \gtrsim t_{\text{eq}}$ , the universe transits to the MD era, resulting in an increase in  $\xi$  and a decrease in  $v$ . It is important to note that the time axis in Fig. 5 is on a logarithmic scale, indicating that the changes in  $\xi$  and  $v$  occur relatively slowly. Nonetheless, this represents a mild nonscaling effect.

When the EMD era occurs,  $\xi$  increases, while  $v$  decreases, and both quantities gradually return to their scaling values after the EMD era ends. Therefore, the EMD era also introduces a nonscaling effect, which will be incorporated into the calculation of the CS loop number density. Furthermore, we estimate the magnitudes of the time derivatives  $\dot{\xi}$  and  $\dot{v}$  by calculating the evolution of their ratios to  $\xi/t$  and  $v/t$ , respectively, as shown in Fig. 6. We find that, during the EMD era for both BPs,  $|t\dot{\xi}/\xi|$  and  $|t\dot{v}/v|$  are smaller than 0.15 and 0.03, respectively. Thus,  $\dot{\xi}$  and  $\dot{v}$  are negligible compared to  $\xi/t$  and  $v/t$ , and this will simplify the calculations below.

Following the derivation from Eq. (29) to Eq. (32), we evaluate the CS loop number density formed during the EMD era as

$$\begin{aligned}
 n_{\text{CS}}^{\text{EMD}}(l, t_1 < t \leq t_2) &= \frac{\mathcal{F}_m \tilde{c}}{t^2} \int_{t_1}^t \frac{v'}{\gamma_{v'} \xi'^3 l'^{1.69} t'^{1.31}} \Theta\left(t' - \frac{l'}{\alpha_m \xi}\right) dt' \\
 &\simeq \frac{\mathcal{F}_m \tilde{c}}{t^2} \left[ -\frac{v'}{0.31 \gamma_{v'} \xi'^3 l'^{1.69} t'^{0.31}} \right]_{t_1}^t + \int_{t_1}^t \frac{v' \delta[t' - l' / (\alpha_m \xi)]}{0.31 \gamma_{v'} \xi'^3 l'^{1.69} t'^{0.31}} dt' \Theta\left(t - \frac{l}{\alpha_m \xi}\right)
 \end{aligned}$$

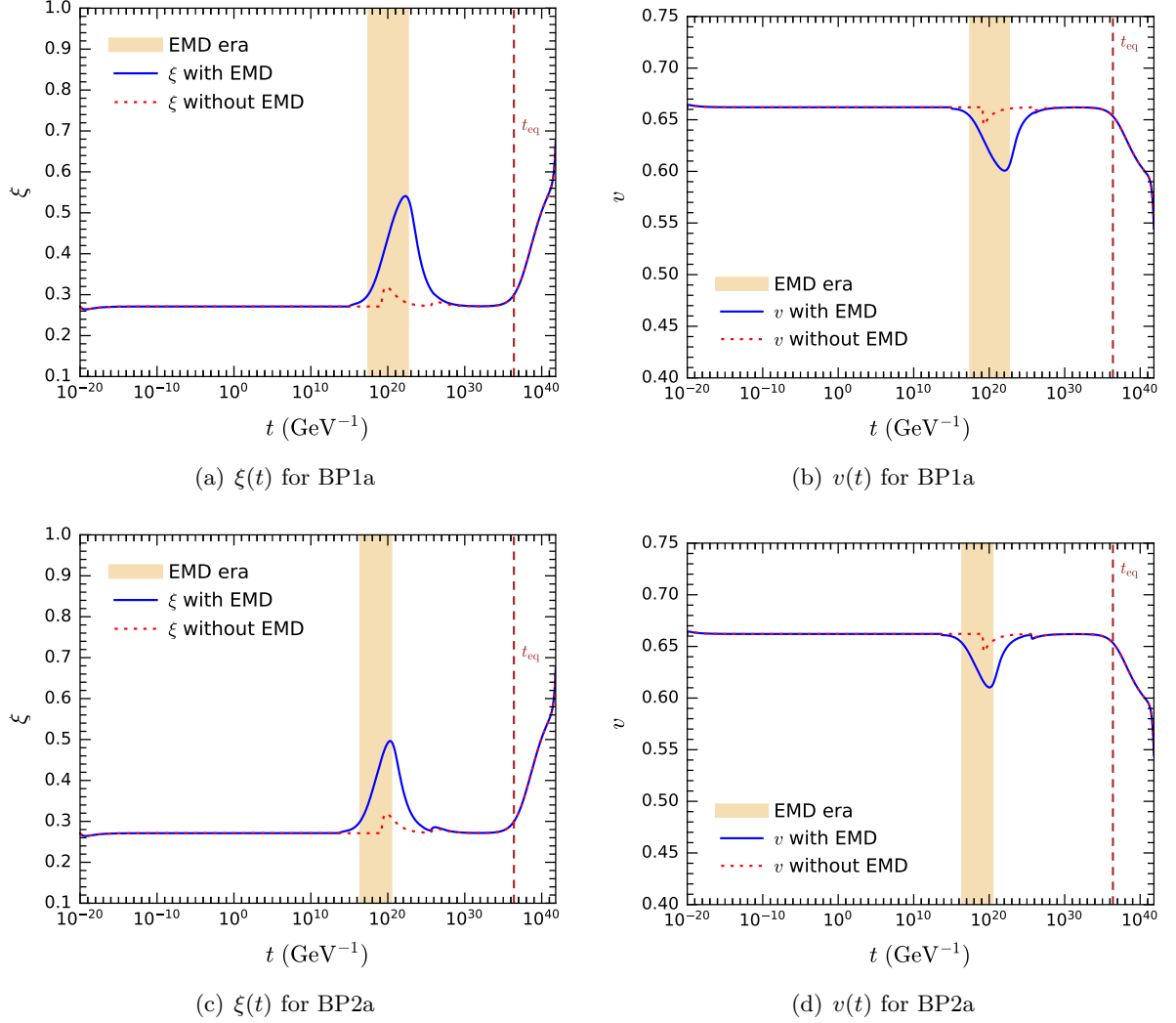


FIG. 5. Evolution of the normalized correlation length  $\xi$  (left panels) and the RMS velocity  $v$  (right panels) of the CS network in the presence of the EMD era (blue solid lines) for BP1a (upper panels) and BP2a (lower panels). The wheat-colored bands denote the duration of the EMD era, while the vertical dashed lines indicate  $t_{\text{eq}}$ . For comparison, the results from the standard  $\Lambda$ CDM model are also plotted as red dotted lines.

$$\begin{aligned}
 &\simeq \frac{\mathcal{F}_m \tilde{c}}{0.31 t^2 (l + \Gamma G \mu t)^2} \left[ \frac{0.18^{0.31} v_\star}{\gamma_{v_\star} \xi_\star^3} - \frac{(l/t)^{0.31} v}{\gamma_v \xi^3} \right] \Theta(0.18t - l) \\
 &\quad + \frac{\mathcal{F}_m \tilde{c} v(t_1) \Theta(0.18t_1 - l - \Gamma G \mu t)}{0.31 \gamma_{v(t_1)} \xi^3(t_1) t_1^2 t^2 [l/t_1 + \Gamma G \mu (t/t_1 - 1)]^{1.69}},
 \end{aligned} \tag{51}$$

where  $\Gamma G \mu \ll \alpha_m \xi_\star = 0.18$  has been used in the third step.

In addition, similar to Eq. (35), we must account for the number densities of CS loops produced in a preceding era and surviving into subsequent eras, with respect to the timeline in Fig. 2. For clarity, we define the notations for these loop number densities as follows.

- $n_{\text{CS}}^{\text{rm}*}$ : CS loops formed in the original RD era and surviving into the EMD era.
- $n_{\text{CS}}^{\text{mr}}$ : CS loops formed in the EMD era and surviving into the second RD era.

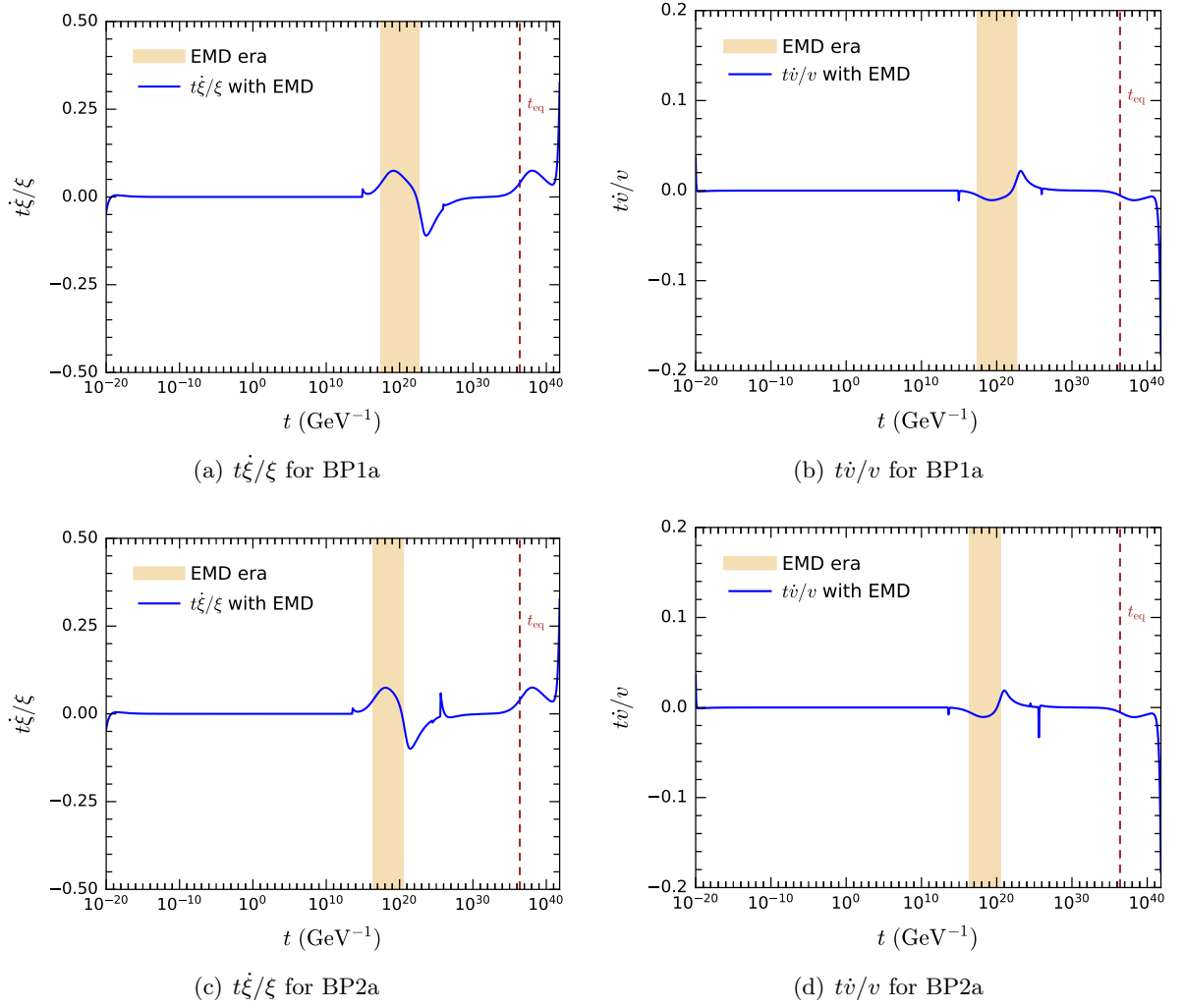


FIG. 6. Evolution of  $t\dot{\xi}/\xi$  (left panels) and  $t\dot{v}/v$  (right panels) in the presence of the EMD era for BP1a (upper panels) and BP2a (lower panels).

- $n_{\text{CS}}^{\text{rm}}$ : CS loops formed in the second RD era and surviving into the final MD era.
- $n_{\text{CS}}^{\text{rmr}}$ : CS loops formed in the original RD era and surviving into the second RD era.
- $n_{\text{CS}}^{\text{mrmm}}$ : CS loops formed in the EMD era and surviving into the final MD era.
- $n_{\text{CS}}^{\text{rmrm}}$ : CS loops formed in the original RD era and surviving into the final MD era.

Following the approach in Ref. [83] for accounting for the cosmological expansion,  $n_{\text{CS}}^{\text{rm}}$  can be determined by

$$n_{\text{CS}}^{\text{rm}}(l, t > t_{\text{eq}})a^3(t) = n_{\text{CS}}^{\text{r}}(l_{\text{eq}}, t_{\text{eq}})a^3(t_{\text{eq}}), \quad (52)$$

where  $l_{\text{eq}} = l + \Gamma G\mu(t - t_{\text{eq}})$ . This leads to

$$n_{\text{CS}}^{\text{rm}}(l, t > t_{\text{eq}}) = \frac{t_{\text{eq}}^2}{t^2} \frac{0.18 \Theta\{0.1t_{\text{eq}} - [l + \Gamma G\mu(t - t_{\text{eq}})]\}}{t_{\text{eq}}^{3/2} (l + \Gamma G\mu t)^{5/2}} \simeq \frac{0.18 t_{\text{eq}}^{1/2} \Theta(0.1t_{\text{eq}} - l - \Gamma G\mu t)}{t^2 (l + \Gamma G\mu t)^{5/2}}, \quad (53)$$

which is just Eq. (35). Similarly, by introducing  $l_{1,2} = l + \Gamma G\mu(t - t_{1,2})$ , we obtain

$$n_{\text{CS}}^{\text{rm}*}(l, t_1 < t \leq t_2) = \frac{a^3(t_1)}{a^3(t)} n_{\text{CS}}^{\text{r}}(l_1, t_1) \simeq \frac{0.18 t_1^{1/2} \Theta(0.1t_1 - l - \Gamma G\mu t)}{t^2 (l + \Gamma G\mu t)^{5/2}}, \quad (54)$$

$$n_{\text{CS}}^{\text{rmr}}(l, t_2 < t \leq t_{\text{eq}}) = \frac{a^3(t_2)}{a^3(t)} n_{\text{CS}}^{\text{rm}*}(l_2, t_2) \simeq \frac{0.18 t_1^{1/2} \Theta(0.1t_1 - l - \Gamma G\mu t)}{t_2^{1/2} t^{3/2} (l + \Gamma G\mu t)^{5/2}}, \quad (55)$$

$$n_{\text{CS}}^{\text{rmrm}}(l, t > t_{\text{eq}}) = \frac{a^3(t_{\text{eq}})}{a^3(t)} n_{\text{CS}}^{\text{rmr}}(l_{\text{eq}}, t_{\text{eq}}) \simeq \frac{0.18 t_1^{1/2} t_{\text{eq}}^{1/2} \Theta(0.1t_1 - l - \Gamma G\mu t)}{t_2^{1/2} t^2 (l + \Gamma G\mu t)^{5/2}}. \quad (56)$$

Moreover, the number densities of CS loops produced during the EMD era and surviving into the second RD and final MD eras are given by

$$\begin{aligned} n_{\text{CS}}^{\text{mr}}(l, t_2 < t \leq t_{\text{eq}}) &= \frac{a^3(t_2)}{a^3(t)} n_{\text{CS}}^{\text{EMD}}(l_2, t_2) \\ &\simeq \frac{\mathcal{F}_m \tilde{c} \Theta(0.18t_2 - l - \Gamma G\mu t)}{0.31 t_2^{1/2} t^{3/2} (l + \Gamma G\mu t)^2} \left[ \frac{0.18^{0.31} v_*}{\gamma_{v_*} \xi_*^3} - \frac{(l_2/t_2)^{0.31} v(t_2)}{\gamma_{v(t_2)} \xi^3(t_2)} \right] \\ &\quad + \frac{\mathcal{F}_m \tilde{c} v(t_1) \Theta(0.18t_1 - l - \Gamma G\mu t)}{0.31 \gamma_{v(t_1)} \xi^3(t_1) t_1^2 t_2^{1/2} t^{3/2} [l/t_1 + \Gamma G\mu(t/t_1 - 1)]^{1.69}}, \end{aligned} \quad (57)$$

$$\begin{aligned} n_{\text{CS}}^{\text{mr}}(l, t > t_{\text{eq}}) &= \frac{a^3(t_{\text{eq}})}{a^3(t)} n_{\text{CS}}^{\text{mr}}(l_{\text{eq}}, t_{\text{eq}}) \\ &\simeq \frac{\mathcal{F}_m \tilde{c} t_{\text{eq}}^{1/2} \Theta(0.18t_2 - l - \Gamma G\mu t)}{0.31 t_2^{1/2} t^2 (l + \Gamma G\mu t)^2} \left[ \frac{0.18^{0.31} v_*}{\gamma_{v_*} \xi_*^3} - \frac{(l_2/t_2)^{0.31} v(t_2)}{\gamma_{v(t_2)} \xi^3(t_2)} \right] \\ &\quad + \frac{\mathcal{F}_m \tilde{c} t_{\text{eq}}^{1/2} v(t_1) \Theta(0.18t_1 - l - \Gamma G\mu t)}{0.31 \gamma_{v(t_1)} \xi^3(t_1) t_1^2 t_2^{1/2} t^2 [l/t_1 + \Gamma G\mu(t/t_1 - 1)]^{1.69}}. \end{aligned} \quad (58)$$

#### D. Modification of the GW spectrum

We now analyze the SGWB spectrum generated by cosmic strings, incorporating modifications to the scale factor  $a(t)$  and the CS loop number density  $n_{\text{CS}}(l, t)$  induced by the EMD era. Based on Eqs. (7) and (8), the GW spectra for  $G\mu = 10^{-11}$  are presented in Figs. 7(a) and 7(b) for BP1a and BP2a, respectively. The contributions from CS loops formed during different eras are demonstrated separately. Note that, in earlier eras, the CS loops are smaller in length and generate GWs at higher frequencies.

In order to assess the sensitivity of GW detection experiments, we also show the constraints from the North American Nanohertz Observatory for Gravitational Waves (NANOGrav) [90], the European Pulsar Timing Array (EPTA) [91], and the Parkes Pulsar Timing Array (PPTA) [92],

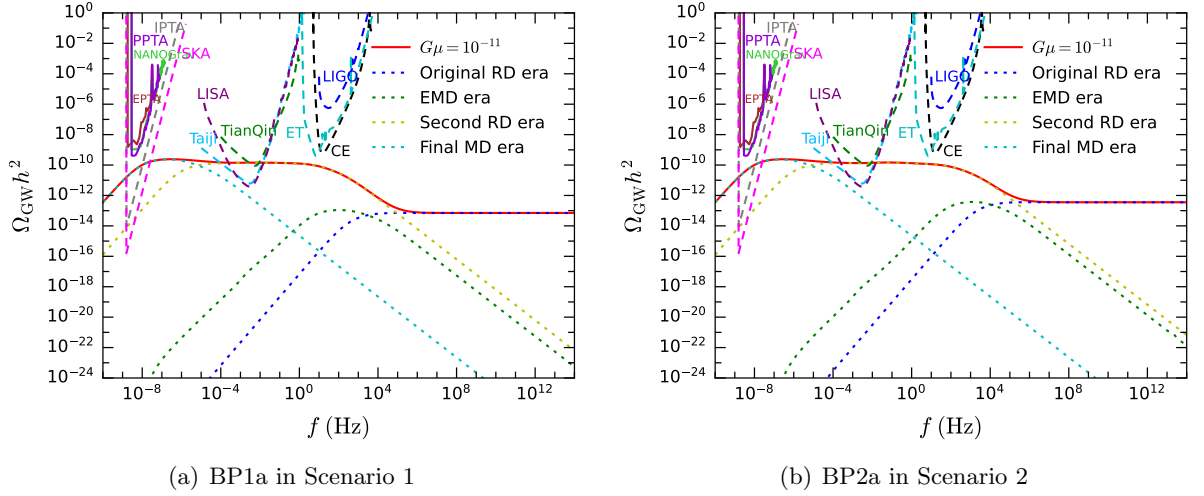


FIG. 7. GW spectra from cosmic strings with  $G\mu = 10^{-11}$  modified by the EMD era for BP1a in Scenario 1 (a) and BP2a in Scenario 2 (b). The red solid lines represent the total GW spectra, which include contributions from CS loops across all eras, while the blue, green, olive, and cyan dotted lines correspond to the contributions from CS loops formed during the original RD, EMD, second RD, and final MD eras, respectively. For comparison, various constraints and sensitivity curves from several GW detection experiments are also shown.

as well as the sensitivity curves of the International Pulsar Timing Array (IPTA) [93], the Square Kilometer Array (SKA) [94], the Laser Interferometer Space Antenna (LISA) [52], TianQin [95], Taiji [96], LIGO [97], the Cosmic Explorer (CE) [98], and the Einstein Telescope (ET) [99].

Compared to the GW spectrum for  $G\mu = 10^{-11}$  in the  $\Lambda$ CDM model illustrated in Fig. 1, the spectra in both BPs with the EMD era display a suppression at high frequencies  $f \gtrsim 10$  Hz, which corresponds to the contributions from CS loops formed during the original RD and EMD eras. The primary reason for this suppression is as follows. Since the scaling behavior of the CS network is only slightly violated, the correlation length  $L$  remains approximately proportional to the cosmic time  $t$ , suggesting that the lengths of the generated loops are positively correlated with the scale factor  $a(t)$ . As shown in Fig. 4, the EMD era reduces the scale factor before  $t_2$ . This means that CS loops with a given initial length  $l$ , which is inversely proportional to the frequencies of the emitted GWs through  $f_e = 2n/l$ , are formed at a later time, when the energy densities of both CS loops and emitted GWs are reduced. As a result, the GW spectrum at sufficiently high frequencies is suppressed, and the end time of the EMD era,  $t_2$ , is related to the GW frequency at which this suppression effect becomes significant. For the parameters listed in Table I, the dilutor  $N_2$  in BP1a has a longer lifetime than the dilutor  $\Delta$  in BP2a, resulting in a longer EMD era and, consequently, a stronger suppression.

We proceed to investigate how the GW spectrum changes with different parameters. In Fig. 8, the GW spectra for BP1a and BP2a are displayed with the CS tension parameter varying as  $G\mu = 10^{-9}$ ,  $10^{-11}$ ,  $3 \times 10^{-13}$ ,  $10^{-15}$ , and  $5 \times 10^{-18}$ . For a smaller CS tension, the GW emission power is reduced, and the lifetimes of CS loops are extended. This suggests that the loops existing at  $t_2$  originated from earlier times with smaller initial lengths, reducing the average loop length

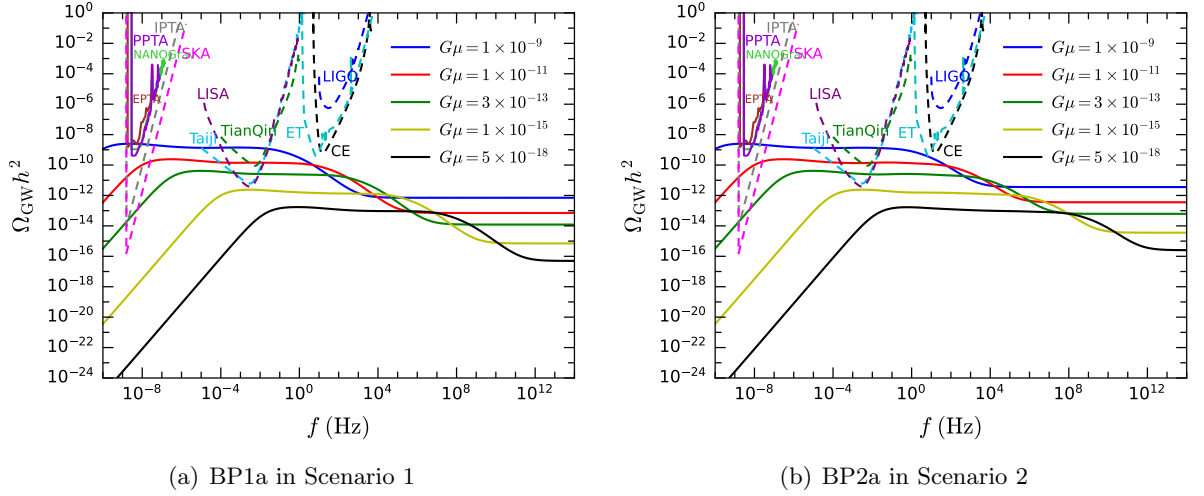


FIG. 8. GW spectra modified by the EMD era for BP1a in Scenario 1 (a) and BP2a in Scenario 2 (b) assuming different values of the CS tension parameter  $G\mu$ .

at  $t_2$  and increasing the frequencies of the emitted GWs. Consequently, the suppression effect caused by the EMD era begins at a higher GW frequency, as shown in Fig. 8.

In addition, we consider the results for BP1b and BP1c in Scenario 1 and for BP2b and BP2c in Scenario 2, whose parameters as tabulated in Tables I and II, respectively. The obtained GW spectra are illustrated in Fig. 9. For BP1a, BP1b, and BP1c in Scenario 1, the dilutor  $N_2$  has the same mass, but the masses of the DM candidate  $N_1$  differ, causing variations in the decay width of  $N_2$ . A smaller decay width  $\Gamma_{N_2}$  corresponds to a longer duration of the EMD era, leading to stronger suppression effects at high frequencies, as illustrated in Fig. 9(a). On the other hand, the masses of the dilutor  $\Delta$  are different for BP2a, BP2b, and BP2c in Scenario 2. A heavier  $\Delta$  implies that the EMD era occurs earlier, and hence a higher frequency at which the suppression of the GW spectrum commences. This is clearly demonstrated in Fig. 9(b).

Furthermore, we assess the influence of the suppression effect caused by the EMD era on the experimental sensitivity of ground-based interferometers. Given a GW spectrum  $\Omega_{\text{noise}}(f)$  converted from the strain noise of a interferometer system, along with a signal spectrum  $\Omega_{\text{signal}}(f)$ , the signal-to-noise ratio (SNR) for a practical observational time  $t_{\text{obs}}$  can be evaluated as [100, 101]

$$\varrho = \left\{ t_{\text{obs}} \int_{f_{\min}}^{f_{\max}} \left[ \frac{\Omega_{\text{signal}}(f)}{\Omega_{\text{noise}}(f)} \right]^2 df \right\}^{1/2}, \quad (59)$$

where  $[f_{\min}, f_{\max}]$  is the accessible frequency band. If the SNR reaches a threshold  $\varrho_{\text{thr}} = 10$ , it is probable that the GW signal will be detected.

Using the sensitivity curves of LIGO, CE, and ET, we compute the SNRs for  $t_{\text{obs}} = 1$  yr as functions of the CS tension parameter  $G\mu$ . The results with the EMD era for BP1a in Scenario 1 and BP2a in Scenario 2 are presented by solid lines in Figs. 10(a) and 10(b), respectively, while those for the  $\Lambda$ CDM model are indicated by dotted lines. In addition, the upper limits

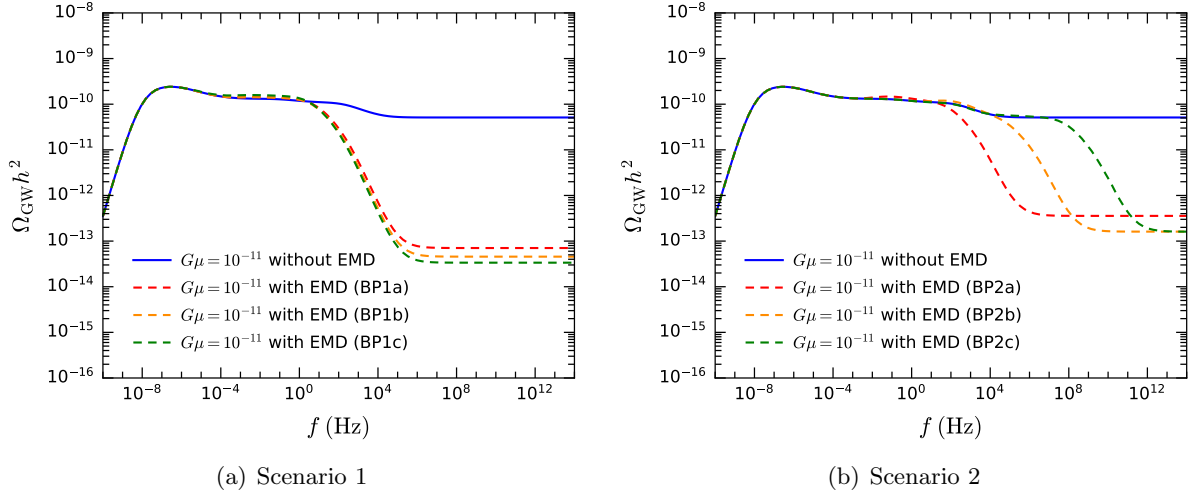


FIG. 9. GW spectra with  $G\mu = 1 \times 10^{-11}$  modified by the EMD era for various BPs in Scenarios 1 (a) and 2 (b). The blue solid lines represents the corresponding GW spectrum in the standard  $\Lambda$ CDM model without the EMD era.

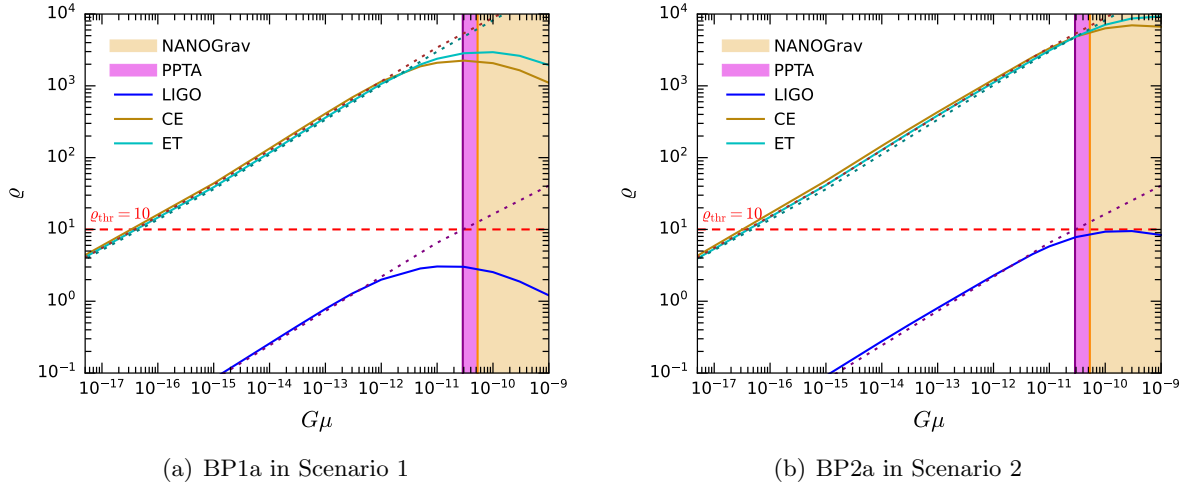


FIG. 10. Estimated SNRs of the LIGO (blue solid lines), CE (gold solid lines), and ET (cyan solid lines) experiments affected by the EMD era for BP1a in Scenario 1 (a) and BP2a in Scenario 2 (b). For comparison, the corresponding SNRs for the  $\Lambda$ CDM models are represented by dotted lines in similar colors.

$G\mu < 5.3 \times 10^{-11}$  and  $G\mu < 2.88 \times 10^{-11}$  at 95% confidence level given by NANOGrav [90] and PPTA [102] searches for a SGWB generated by cosmic strings are indicated by the regions shaded in wheat and magenta colors. For the BPs we choose, the EMD era does not influence the GW spectrum in the  $\sim$  nHz frequency band, where the PTA experiments are sensitive, and thus these upper limits remain valid.

For  $G\mu \lesssim 10^{-12}$ , we find that the inclusion of the EMD era has insignificant impact on the SNRs, because the suppression effect occurs at frequencies outside the sensitive bands of LIGO, CE, and ET (cf. Fig. 8). In contrast, for  $G\mu \gtrsim 10^{-12}$ , the SNRs are obviously reduced. Compared to BP2a, the dilutor in BP1a has a longer lifetime, leading to a stronger suppression

effect and, consequently, smaller SNRs.

#### IV. SUMMARY

In this work, we explore the influence of an EMD era on the dynamics of a preexisting CS network and the resulting SGWB. We first review the GWs generated by CS loops, highlighting the explicit dependence of the SGWB spectrum on the CS loop number density  $n_{\text{CS}}$  and the scale factor  $a(t)$ . We then analyze the evolution of the CS network based on the VOS model and discuss the scaling behavior. By assuming appropriate forms for the loop production functions, we derive expressions for the CS loop number densities in RD and MD eras, which are consistent with numerical simulations in the scaling regime. Notably, these expressions are expected to remain valid even in cases where the scaling behavior is violated.

Next, we consider a cosmic timeline that incorporates an EMD era within the conventional RD era. As an illustrative example, this EMD era is attributed to a massive, long-lived dilutor in the DM dilution mechanism, particularly within the framework of the minimal LRSM, where the dilutor is either  $N_2$  in Scenario 1 or  $\Delta$  in Scenario 2. In this context, the overproduction of the DM particle  $N_1$  is resolved by entropy injection from the dilutor decays. By solving the Boltzmann equations, we obtain the evolution of the number densities for the dilutor, DM, and SM particles, as well as the time dependence of the scale factor. These solutions allow us to identify the onset and conclusion of the EMD era. Compared to the standard  $\Lambda$ CDM cosmological model, the scale factor before the end time  $t_2$  of the EMD era is smaller.

Furthermore, we show that the evolution of the normalized correlation length  $\xi$  and the RMS velocity  $v$  of the CS network is modified by the presence of the EMD era, exhibiting a nonscaling behavior. Subsequently, we calculate the number density of CS loops formed during the EMD era, as well as the number densities of loops generated in earlier eras and surviving into later eras. Using these results, the influence of the EMD era on the SGWB spectrum arising from CS loops is demonstrated.

We find that the EMD era induces a suppression in the SGWB spectrum at sufficiently high frequencies, which is linked to the reduction of the scale factor prior to  $t_2$ . Additionally, for a smaller CS tension, the average length of CS loops at  $t_2$  is smaller, causing the suppression effect to begin at a higher frequency. Moreover, a smaller decay width of the dilutor implies a longer duration of the EMD era, leading to a stronger suppression effect. Furthermore, a heavier dilutor causes an EMD era to occur earlier, resulting in suppression at higher frequencies.

Finally, we estimate the SNRs of the ground-based interferometers LIGO, CE, and ET as functions of  $G\mu$ . The results show that for BP1a and BP1b with  $G\mu \gtrsim 10^{-12}$ , the SNRs are significantly reduced, as the suppression effect falls within the sensitive frequency bands of these experiments. This study highlights that changes in the cosmic history, such as the presence of an EMD era, can affect the dynamics of the CS network and produce observable signatures in the resulting SGWB spectrum.

## ACKNOWLEDGMENTS

The authors acknowledge Ye-Ling Zhou for helpful discussions. This work is supported by the Guangzhou Science and Technology Planning Project under Grant No. 2024A04J4026.

- 
- [1] G. Gamow, “Expanding universe and the origin of elements,” *Phys. Rev.* **70** (1946) 572–573.
  - [2] E. Hubble, “A relation between distance and radial velocity among extra-galactic nebulae,” *Proc. Nat. Acad. Sci.* **15** (1929) 168–173.
  - [3] R. V. Wagoner, W. A. Fowler, and F. Hoyle, “On the Synthesis of elements at very high temperatures,” *Astrophys. J.* **148** (1967) 3–49.
  - [4] B. D. Fields, K. A. Olive, T.-H. Yeh, and C. Young, “Big-Bang Nucleosynthesis after Planck,” *JCAP* **03** (2020) 010, [arXiv:1912.01132 \[astro-ph.CO\]](#). [Erratum: *JCAP* **11**, E02 (2020)].
  - [5] A. A. Penzias and R. W. Wilson, “A Measurement of excess antenna temperature at 4080-Mc/s,” *Astrophys. J.* **142** (1965) 419–421.
  - [6] **COBE** Collaboration, G. F. Smoot *et al.*, “Structure in the COBE differential microwave radiometer first year maps,” *Astrophys. J. Lett.* **396** (1992) L1–L5.
  - [7] **WMAP** Collaboration, G. Hinshaw *et al.*, “Nine-Year Wilkinson Microwave Anisotropy Probe (WMAP) Observations: Cosmological Parameter Results,” *Astrophys. J. Suppl.* **208** (2013) 19, [arXiv:1212.5226 \[astro-ph.CO\]](#).
  - [8] **Planck** Collaboration, N. Aghanim *et al.*, “Planck 2018 results. VI. Cosmological parameters,” *Astron. Astrophys.* **641** (2020) A6, [arXiv:1807.06209 \[astro-ph.CO\]](#). [Erratum: *Astron. Astrophys.* **652**, C4 (2021)].
  - [9] **Supernova Search Team** Collaboration, A. G. Riess *et al.*, “Observational evidence from supernovae for an accelerating universe and a cosmological constant,” *Astron. J.* **116** (1998) 1009–1038, [arXiv:astro-ph/9805201](#).
  - [10] **Supernova Cosmology Project** Collaboration, S. Perlmutter *et al.*, “Measurements of  $\Omega$  and  $\Lambda$  from 42 High Redshift Supernovae,” *Astrophys. J.* **517** (1999) 565–586, [arXiv:astro-ph/9812133](#).
  - [11] R. Allahverdi *et al.*, “The First Three Seconds: a Review of Possible Expansion Histories of the Early Universe,” [arXiv:2006.16182 \[astro-ph.CO\]](#).
  - [12] A. G. Polnarev and M. Y. Khlopov, “The ERA of Superheavy Particle Dominance and Big Bang Nucleosynthesis,” *Astron. Zh.* **59** (1982) 15–19. [English translation: *Sov. Astron.* **26** (1982) 9–12].
  - [13] J. McDonald, “WIMP Densities in Decaying Particle Dominated Cosmology,” *Phys. Rev. D* **43** (1991) 1063–1068.
  - [14] H. Assadullahi and D. Wands, “Gravitational waves from an early matter era,” *Phys. Rev. D* **79** (2009) 083511, [arXiv:0901.0989 \[astro-ph.CO\]](#).
  - [15] A. L. Erickcek, “The Dark Matter Annihilation Boost from Low-Temperature Reheating,” *Phys. Rev. D* **92** (2015) 103505, [arXiv:1504.03335 \[astro-ph.CO\]](#).
  - [16] A. E. Nelson and H. Xiao, “Axion Cosmology with Early Matter Domination,” *Phys. Rev. D* **98** (2018) 063516, [arXiv:1807.07176 \[astro-ph.CO\]](#).
  - [17] M. Cirelli, Y. Gouttenoire, K. Petraki, and F. Sala, “Homeopathic Dark Matter, or how diluted heavy substances produce high energy cosmic rays,” *JCAP* **02** (2019) 014, [arXiv:1811.03608 \[hep-ph\]](#).
  - [18] P. Chattopadhyay, A. Chaudhuri, and M. Y. Khlopov, “Dark matter from evaporating primordial

- black holes in the early universe,” *Int. J. Geom. Meth. Mod. Phys.* **22** (2025) 2450251, [arXiv:2209.11288 \[hep-ph\]](#).
- [19] A. Banerjee, D. Chowdhury, A. Hait, and M. S. Islam, “Dark matter cooling during early matter-domination boosts sub-earth halos,” [arXiv:2408.08360 \[astro-ph.CO\]](#).
- [20] B. Spokoiny, “Deflationary universe scenario,” *Phys. Lett. B* **315** (1993) 40–45, [arXiv:gr-qc/9306008](#).
- [21] M. Joyce, “Electroweak Baryogenesis and the Expansion Rate of the Universe,” *Phys. Rev. D* **55** (1997) 1875–1878, [arXiv:hep-ph/9606223](#).
- [22] P. G. Ferreira and M. Joyce, “Cosmology with a primordial scaling field,” *Phys. Rev. D* **58** (1998) 023503, [arXiv:astro-ph/9711102](#).
- [23] R. T. Co, D. Dunsy, N. Fernandez, A. Ghalsasi, L. J. Hall, K. Harigaya, and J. Shelton, “Gravitational wave and CMB probes of axion kination,” *JHEP* **09** (2022) 116, [arXiv:2108.09299 \[hep-ph\]](#).
- [24] Y. Gouttenoire, G. Servant, and P. Simakachorn, “Kination cosmology from scalar fields and gravitational-wave signatures,” [arXiv:2111.01150 \[hep-ph\]](#).
- [25] A. Ghoshal, L. Heurtier, and A. Paul, “Signatures of non-thermal dark matter with kination and early matter domination. Gravitational waves versus laboratory searches,” *JHEP* **12** (2022) 105, [arXiv:2208.01670 \[hep-ph\]](#).
- [26] J. Silk and M. S. Turner, “Double Inflation,” *Phys. Rev. D* **35** (1987) 419.
- [27] D. H. Lyth and E. D. Stewart, “Thermal inflation and the moduli problem,” *Phys. Rev. D* **53** (1996) 1784–1798, [arXiv:hep-ph/9510204](#).
- [28] P. Creminelli, A. Nicolis, and R. Rattazzi, “Holography and the electroweak phase transition,” *JHEP* **03** (2002) 051, [arXiv:hep-th/0107141](#).
- [29] T. Konstandin and G. Servant, “Cosmological Consequences of Nearly Conformal Dynamics at the TeV scale,” *JCAP* **12** (2011) 009, [arXiv:1104.4791 \[hep-ph\]](#).
- [30] **LIGO Scientific, Virgo** Collaboration, B. P. Abbott *et al.*, “Observation of Gravitational Waves from a Binary Black Hole Merger,” *Phys. Rev. Lett.* **116** (2016) 061102, [arXiv:1602.03837 \[gr-qc\]](#).
- [31] Y. Cui, M. Lewicki, D. E. Morrissey, and J. D. Wells, “Cosmic Archaeology with Gravitational Waves from Cosmic Strings,” *Phys. Rev. D* **97** (2018) 123505, [arXiv:1711.03104 \[hep-ph\]](#).
- [32] Y. Cui, M. Lewicki, D. E. Morrissey, and J. D. Wells, “Probing the pre-BBN universe with gravitational waves from cosmic strings,” *JHEP* **01** (2019) 081, [arXiv:1808.08968 \[hep-ph\]](#).
- [33] G. S. F. Guedes, P. P. Avelino, and L. Sousa, “Signature of inflation in the stochastic gravitational wave background generated by cosmic string networks,” *Phys. Rev. D* **98** (2018) 123505, [arXiv:1809.10802 \[astro-ph.CO\]](#).
- [34] N. Ramberg and L. Visinelli, “Probing the Early Universe with Axion Physics and Gravitational Waves,” *Phys. Rev. D* **99** (2019) 123513, [arXiv:1904.05707 \[astro-ph.CO\]](#).
- [35] P. Auclair *et al.*, “Probing the gravitational wave background from cosmic strings with LISA,” *JCAP* **04** (2020) 034, [arXiv:1909.00819 \[astro-ph.CO\]](#).
- [36] C.-F. Chang and Y. Cui, “Stochastic Gravitational Wave Background from Global Cosmic Strings,” *Phys. Dark Univ.* **29** (2020) 100604, [arXiv:1910.04781 \[hep-ph\]](#).
- [37] Y. Gouttenoire, G. Servant, and P. Simakachorn, “Beyond the Standard Models with Cosmic Strings,” *JCAP* **07** (2020) 032, [arXiv:1912.02569 \[hep-ph\]](#).
- [38] Y. Gouttenoire, G. Servant, and P. Simakachorn, “BSM with Cosmic Strings: Heavy, up to EeV mass, Unstable Particles,” *JCAP* **07** (2020) 016, [arXiv:1912.03245 \[hep-ph\]](#).
- [39] C.-F. Chang and Y. Cui, “Gravitational waves from global cosmic strings and cosmic

- archaeology,” *JHEP* **03** (2022) 114, [arXiv:2106.09746 \[hep-ph\]](#).
- [40] F. Muia, F. Quevedo, A. Schachner, and G. Villa, “Testing BSM physics with gravitational waves,” *JCAP* **09** (2023) 006, [arXiv:2303.01548 \[hep-ph\]](#).
- [41] Z.-Y. Qiu and Z.-H. Yu, “Gravitational waves from cosmic strings associated with pseudo-Nambu-Goldstone dark matter\*,” *Chin. Phys. C* **47** (2023) 085104, [arXiv:2304.02506 \[hep-ph\]](#).
- [42] A. Ghoshal, Y. Gouttenoire, L. Heurtier, and P. Simakachorn, “Primordial black hole archaeology with gravitational waves from cosmic strings,” *JHEP* **08** (2023) 196, [arXiv:2304.04793 \[hep-ph\]](#).
- [43] H. B. Nielsen and P. Olesen, “Vortex Line Models for Dual Strings,” *Nucl. Phys. B* **61** (1973) 45–61.
- [44] T. W. B. Kibble, “Topology of Cosmic Domains and Strings,” *J. Phys. A* **9** (1976) 1387–1398.
- [45] D. P. Bennett and F. R. Bouchet, “Cosmic string evolution,” *Phys. Rev. Lett.* **63** (1989) 2776.
- [46] A. Albrecht and N. Turok, “Evolution of Cosmic String Networks,” *Phys. Rev. D* **40** (1989) 973–1001.
- [47] D. P. Bennett and F. R. Bouchet, “High resolution simulations of cosmic string evolution. 1. Network evolution,” *Phys. Rev. D* **41** (1990) 2408.
- [48] B. Allen and E. P. S. Shellard, “Cosmic string evolution: a numerical simulation,” *Phys. Rev. Lett.* **64** (1990) 119–122.
- [49] F. Jenet *et al.*, “The North American Nanohertz Observatory for Gravitational Waves,” [arXiv:0909.1058 \[astro-ph.IM\]](#).
- [50] **EPTA** Collaboration, M. Kramer and D. J. Champion, “The European Pulsar Timing Array and the Large European Array for Pulsars,” *Class. Quant. Grav.* **30** (2013) 224009.
- [51] **IPTA** Collaboration, M. Falxa *et al.*, “Searching for continuous Gravitational Waves in the second data release of the International Pulsar Timing Array,” *Mon. Not. Roy. Astron. Soc.* **521** (2023) 5077–5086, [arXiv:2303.10767 \[gr-qc\]](#).
- [52] **LISA** Collaboration, P. Amaro-Seoane *et al.*, “Laser Interferometer Space Antenna,” [arXiv:1702.00786 \[astro-ph.IM\]](#).
- [53] Chiummo, Antonino, “The Einstein Telescope: Status of the project,” *EPJ Web Conf.* **280** (2023) 03003.
- [54] **TianQin** Collaboration, J. Luo *et al.*, “TianQin: a space-borne gravitational wave detector,” *Class. Quant. Grav.* **33** (2016) 035010, [arXiv:1512.02076 \[astro-ph.IM\]](#).
- [55] W.-R. Hu and Y.-L. Wu, “The Taiji Program in Space for gravitational wave physics and the nature of gravity,” *National Science Review* **4** (10, 2017) 685–686, <https://academic.oup.com/nsr/article-pdf/4/5/685/31566708/nwx116.pdf>.
- [56] **LIGO Scientific** Collaboration, J. Aasi *et al.*, “Advanced LIGO,” *Class. Quant. Grav.* **32** (2015) 074001, [arXiv:1411.4547 \[gr-qc\]](#).
- [57] **VIRGO** Collaboration, F. Acernese *et al.*, “Advanced Virgo: a second-generation interferometric gravitational wave detector,” *Class. Quant. Grav.* **32** (2015) 024001, [arXiv:1408.3978 \[gr-qc\]](#).
- [58] D. Reitze *et al.*, “Cosmic Explorer: The U.S. Contribution to Gravitational-Wave Astronomy beyond LIGO,” *Bull. Am. Astron. Soc.* **51** (2019) 035, [arXiv:1907.04833 \[astro-ph.IM\]](#).
- [59] A. G. Doroshkevich and M. Y. Khlopov, “Grand Unification Cosmology and the Parameters of a Neutrino Dominated Universe,” *Pis'ma Astron. Zh.* **9** (1983) 323–326. [English translation: *Sov. Astron. Lett.* **9** (1983) no. 3, 171–173].
- [60] E. A. Baltz and H. Murayama, “Gravitino warm dark matter with entropy production,” *JHEP* **05** (2003) 067, [arXiv:astro-ph/0108172](#).

- [61] T. Asaka, M. Shaposhnikov, and A. Kusenko, “Opening a new window for warm dark matter,” *Phys. Lett. B* **638** (2006) 401–406, [arXiv:hep-ph/0602150](#).
- [62] J. A. Evans, A. Ghalsasi, S. Gori, M. Tammaro, and J. Zupan, “Light Dark Matter from Entropy Dilution,” *JHEP* **02** (2020) 151, [arXiv:1910.06319 \[hep-ph\]](#).
- [63] C. Cosme, M. Dutra, T. Ma, Y. Wu, and L. Yang, “Neutrino portal to FIMP dark matter with an early matter era,” *JHEP* **03** (2021) 026, [arXiv:2003.01723 \[hep-ph\]](#).
- [64] P. Chanda and J. Unwin, “Decoupling of asymmetric dark matter during an early matter dominated era,” *JCAP* **06** (2021) 032, [arXiv:2102.02313 \[hep-ph\]](#).
- [65] A. Chaudhuri and M. Y. Khlopov, “Dark matter dilution scenarios in the early universe,” *Int. J. Mod. Phys. D* **30** (2021) 2140008, [arXiv:2110.15854 \[hep-ph\]](#).
- [66] P. Asadi, T. R. Slatyer, and J. Smirnov, “WIMPs without weakness: Generalized mass window with entropy injection,” *Phys. Rev. D* **106** (2022) 015012, [arXiv:2111.11444 \[hep-ph\]](#).
- [67] M. Nemevšek and Y. Zhang, “Dark Matter Dilution Mechanism through the Lens of Large-Scale Structure,” *Phys. Rev. Lett.* **130** (2023) 121002, [arXiv:2206.11293 \[hep-ph\]](#).
- [68] M. Nemevšek and Y. Zhang, “Anatomy of diluted dark matter in the minimal left-right symmetric model,” *Phys. Rev. D* **109** (2024) 056021, [arXiv:2312.00129 \[hep-ph\]](#).
- [69] M. B. Hindmarsh and T. W. B. Kibble, “Cosmic strings,” *Rept. Prog. Phys.* **58** (1995) 477–562, [arXiv:hep-ph/9411342](#).
- [70] M. Maggiore, *Gravitational Waves. Vol. 2: Astrophysics and Cosmology*. Oxford University Press, 3, 2018.
- [71] B. Allen and E. P. S. Shellard, “Gravitational radiation from cosmic strings,” *Phys. Rev. D* **45** (1992) 1898–1912.
- [72] A. Vilenkin and E. P. S. Shellard, *Cosmic Strings and Other Topological Defects*. Cambridge University Press, 7, 2000.
- [73] T. Vachaspati and A. Vilenkin, “Gravitational Radiation from Cosmic Strings,” *Phys. Rev. D* **31** (1985) 3052.
- [74] J. J. Blanco-Pillado and K. D. Olum, “Stochastic gravitational wave background from smoothed cosmic string loops,” *Phys. Rev. D* **96** (2017) 104046, [arXiv:1709.02693 \[astro-ph.CO\]](#).
- [75] P. Binetruy, A. Bohe, C. Caprini, and J.-F. Dufaux, “Cosmological Backgrounds of Gravitational Waves and eLISA/NGO: Phase Transitions, Cosmic Strings and Other Sources,” *JCAP* **06** (2012) 027, [arXiv:1201.0983 \[gr-qc\]](#).
- [76] **Particle Data Group** Collaboration, R. L. Workman *et al.*, “Review of Particle Physics,” *PTEP* **2022** (2022) 083C01.
- [77] C. J. A. P. Martins and E. P. S. Shellard, “String evolution with friction,” *Phys. Rev. D* **53** (1996) 575–579, [arXiv:hep-ph/9507335](#).
- [78] C. J. A. P. Martins and E. P. S. Shellard, “Quantitative string evolution,” *Phys. Rev. D* **54** (1996) 2535–2556, [arXiv:hep-ph/9602271](#).
- [79] C. J. A. P. Martins and E. P. S. Shellard, “Extending the velocity dependent one scale string evolution model,” *Phys. Rev. D* **65** (2002) 043514, [arXiv:hep-ph/0003298](#).
- [80] D. Marfatia and Y.-L. Zhou, “Gravitational waves from cosmic superstrings and gauge strings,” *JHEP* **07** (2024) 204, [arXiv:2312.10455 \[hep-ph\]](#).
- [81] P. Auclair, S. Blasi, V. Brdar, and K. Schmitz, “Gravitational waves from current-carrying cosmic strings,” *JCAP* **04** (2023) 009, [arXiv:2207.03510 \[astro-ph.CO\]](#).
- [82] J. J. Blanco-Pillado, K. D. Olum, and B. Shlaer, “Large parallel cosmic string simulations: New results on loop production,” *Phys. Rev. D* **83** (2011) 083514, [arXiv:1101.5173 \[astro-ph.CO\]](#).
- [83] J. J. Blanco-Pillado, K. D. Olum, and B. Shlaer, “The number of cosmic string loops,” *Phys. Rev.*

- D* **89** (2014) 023512, [arXiv:1309.6637 \[astro-ph.CO\]](#).
- [84] L. Sousa and P. P. Avelino, “Stochastic Gravitational Wave Background generated by Cosmic String Networks: Velocity-Dependent One-Scale model versus Scale-Invariant Evolution,” *Phys. Rev. D* **88** (2013) 023516, [arXiv:1304.2445 \[astro-ph.CO\]](#).
  - [85] E. W. Kolb, *The Early Universe*, vol. 69. Taylor and Francis, 5, 2019.
  - [86] J. R. Ellis, A. D. Linde, and D. V. Nanopoulos, “Inflation Can Save the Gravitino,” *Phys. Lett. B* **118** (1982) 59–64.
  - [87] J. R. Ellis, J. S. Hagelin, D. V. Nanopoulos, K. A. Olive, and M. Srednicki, “Supersymmetric Relics from the Big Bang,” *Nucl. Phys. B* **238** (1984) 453–476.
  - [88] R. N. Mohapatra and J. C. Pati, “A Natural Left-Right Symmetry,” *Phys. Rev. D* **11** (1975) 2558.
  - [89] G. Senjanovic and R. N. Mohapatra, “Exact Left-Right Symmetry and Spontaneous Violation of Parity,” *Phys. Rev. D* **12** (1975) 1502.
  - [90] **NANOGrav** Collaboration, Z. Arzoumanian *et al.*, “The NANOGrav 11-year Data Set: Pulsar-timing Constraints On The Stochastic Gravitational-wave Background,” *Astrophys. J.* **859** (2018) 47, [arXiv:1801.02617 \[astro-ph.HE\]](#).
  - [91] L. Lentati *et al.*, “European Pulsar Timing Array Limits On An Isotropic Stochastic Gravitational-Wave Background,” *Mon. Not. Roy. Astron. Soc.* **453** (2015) 2576–2598, [arXiv:1504.03692 \[astro-ph.CO\]](#).
  - [92] R. M. Shannon *et al.*, “Gravitational waves from binary supermassive black holes missing in pulsar observations,” *Science* **349** (2015) 1522–1525, [arXiv:1509.07320 \[astro-ph.CO\]](#).
  - [93] G. Hobbs *et al.*, “The international pulsar timing array project: using pulsars as a gravitational wave detector,” *Class. Quant. Grav.* **27** (2010) 084013, [arXiv:0911.5206 \[astro-ph.SR\]](#).
  - [94] G. Janssen *et al.*, “Gravitational wave astronomy with the SKA,” *PoS AASKA14* (2015) 037, [arXiv:1501.00127 \[astro-ph.IM\]](#).
  - [95] Z.-C. Liang, Y.-M. Hu, Y. Jiang, J. Cheng, J.-d. Zhang, and J. Mei, “Science with the TianQin Observatory: Preliminary results on stochastic gravitational-wave background,” *Phys. Rev. D* **105** (2022) 022001, [arXiv:2107.08643 \[astro-ph.CO\]](#).
  - [96] W.-H. Ruan, Z.-K. Guo, R.-G. Cai, and Y.-Z. Zhang, “Taiji program: Gravitational-wave sources,” *Int. J. Mod. Phys. A* **35** (2020) 2050075, [arXiv:1807.09495 \[gr-qc\]](#).
  - [97] **KAGRA, LIGO Scientific, Virgo, VIRGO** Collaboration, B. P. Abbott *et al.*, “Prospects for observing and localizing gravitational-wave transients with Advanced LIGO, Advanced Virgo and KAGRA,” *Living Rev. Rel.* **21** (2018) 3, [arXiv:1304.0670 \[gr-qc\]](#).
  - [98] **LIGO Scientific** Collaboration, B. P. Abbott *et al.*, “Exploring the Sensitivity of Next Generation Gravitational Wave Detectors,” *Class. Quant. Grav.* **34** (2017) 044001, [arXiv:1607.08697 \[astro-ph.IM\]](#).
  - [99] S. Hild *et al.*, “Sensitivity Studies for Third-Generation Gravitational Wave Observatories,” *Class. Quant. Grav.* **28** (2011) 094013, [arXiv:1012.0908 \[gr-qc\]](#).
  - [100] E. Thrane and J. D. Romano, “Sensitivity curves for searches for gravitational-wave backgrounds,” *Phys. Rev. D* **88** (2013) 124032, [arXiv:1310.5300 \[astro-ph.IM\]](#).
  - [101] K. Schmitz, “New Sensitivity Curves for Gravitational-Wave Signals from Cosmological Phase Transitions,” *JHEP* **01** (2021) 097, [arXiv:2002.04615 \[hep-ph\]](#).
  - [102] L. Bian, J. Shu, B. Wang, Q. Yuan, and J. Zong, “Searching for cosmic string induced stochastic gravitational wave background with the Parkes Pulsar Timing Array,” *Phys. Rev. D* **106** (2022) L101301, [arXiv:2205.07293 \[hep-ph\]](#).